Commercial Pt/C nanoparticle catalyst enhancement by ionic liquid (IL)/organic ionic plastic crystal (OIPC) modification for oxidation of biofuels in fuel cells.

By

©Abhishek Rameshwar Suryawanshi

B.Sc., Mumbai University, India, 2019

A thesis submitted to the School of Graduate Studies in partial fulfillment of the requirement
for the degree of

Master of Science

Department of Chemistry │ Faculty of Science

Memorial University of Newfoundland

St. John's, NL

September 2021

Abstract

Due to rising environmental concerns, carbon neutral or carbon negative strategies are being sought along with a wide range of clean energy conversion technologies, such as fuel cells. Fuel cells are being investigated owing to their low emissions, high theoretical efficiency, and simplicity of operation. A significant barrier to fuel cell commercialization is cost, mainly due to the use of expensive noble metals as catalysts, e.g., Pt. One strategy would still rely on Pt as a catalyst material but with electrocatalytic enhancement by OIPC (organic ionic plastic crystal) or IL (ionic liquid) modification which lowers the amount of Pt needed. IL are large organic salts with melting points below 100 °C, while OIPC are chemically similar; however, they have higher melting points with several solid-solid phase transitions below the melt which give rise to their plasticity. Solid catalyst with an ionic liquid layer (SCILL) is the concept of catalyst modification with a thin IL layer and has been demonstrated as a facile approach to improve catalyst activity. IL/OIPC modified 20% mass Pt/C nanoparticles were investigated as an anodic catalyst for proton exchange membrane fuel cells through oxidation of different biofuels such as methanol and formic acid (FA). Herein, three different tetraalkylphosphonium cations were paired with the bis(trifluoromethylsulfonyl)imide (NTf_2) anion. Three n-butyl group were employed, while the fourth arm bound to the phosphonium core was varied in length from 4 to 8 carbons. Each gave excellent hydrophobicity as well as thermal and electrochemical stability. Tetrabutylphosphonium bis(trifluoromethylsulfonyl) imide ($P_{4444}NTf_2$) possesses a melting point of 85 °C and a single solid-solid phase transition was observed below this temperature, making it an OIPC, while the other salts were liquids at room temperature. As evidenced through voltammetric analysis, commercial 20% Pt/C catalysts demonstrated enhanced organic fuel oxidation when modified by either IL or OIPC of up to 2.5×. These results are highly significant and mean a reduction in the

amount of Pt needed – an enormous cost savings. IL/OIPC physicochemical characterization will also be discussed.

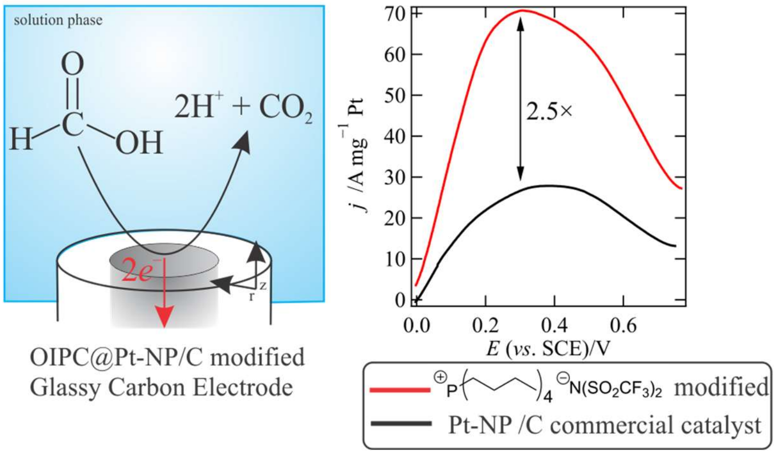

Acknowledgements

Foremost, I would like to express my sincere gratitude to my supervisors; Dr. Peter G. Pickup, his immense knowledge and experience have encouraged me in all the time of academic research and Dr. Talia J. Stockmann for her invaluable supervision, support, profound expertise.

My sincere thanks to my committee member Dr. Graham J. Bodwell for his guidance. Many thanks to Dr. Yuming Zhao for his advice, feedback, and kind support. This project would have not been possible without the assistance of my colleagues Hui, Nazanin, Reza, Ahmed, Diala, Qi, Siamak and Jasmeen.

I would also like to express gratitude to Stephanie Tucker and Chris Corkum from Electron microscopy for their expertise during TEM analysis, Dr. Jian-Bin Lin for training me on various instruments. I acknowledge the support staff Debbie, Mary, and Ann Marie Pike for their assistance and technical aid. I am grateful to work with Nick Ryan and Tiber Reardon during my TA sessions. I would like to extend my sincere gratitude to the funding agencies NSERC and School of Graduate Studies for their support in making my program a reality

My sincere thanks to my undergraduate supervisor Dr. Paresh Gaikar who introduced me in the field of research and finally, I'd like to convey my heartfelt gratitude to my parents and friends for their unwavering support.

Once again, I thank my supervisors for giving me the opportunity to be a part of the team, you will always be an inspiration for me.

Contents

List of Tables

List of Figures

List of Abbreviations

Abbreviation	Description
AFC	Alkaline fuel cell
CO	Carbon monoxide
CV	Cyclic voltammetry
DSC	Differential scanning calorimeter
DAFC	Direct alcohol fuel cell
DEFC	Direct ethanol fuel cell
EV	Electric vehicle
ECSA	Electrocatalytic surface area
EDX	Energy Dispersive X-ray
EEA	European environmental agency
FA	Formic acid
FC	Fuel cell
FCV	Fuel cell vehicles
GE	General electric
GCE	Glassy carbon electrode
GHG	Greenhouse gas
ICPMS	Inductively coupled plasma mass spectrometry
IL	Ionic liquid
Li-ion	Lithium ion
MRI	Magnetic resonance imaging

MOR	Methanol oxidation reaction
MCFC	Molten carbonate fuel cell
NPs	Nanoparticles
NASA	National Aeronautics and Space Administration
NO_x	Nitrogen oxides
NRR	Nitrogen reduction reaction
OIPC	Organic ionic plastic crystal
PAFC	Phosphoric acid fuel cell
PBI	Polybenzimidazole
PEMFC	Polymer electrolyte membrane fuel cell
PVA	Polyvinyl alcohol
PEM	Proton exchange membrane
RTIL	Room temperature ionic liquid
RDE	Rotating disk electrode
SECM	scanning electrochemical microscopy
SEM	Scanning Electron Microscopy
SCILL	Solid catalyst with ionic liquid layer
SC-OIPC	Solid catalyst with organic ionic plastic crystal layer
SOFC	Solid oxide fuel cell
SPEEK	Sulfonated polyether ether ketone
TGA	Thermogravimetric analysis
TEM	Transmission electron microscopy
USDE	U.S. Department of Energy

Chapter 1

1.1 Introduction

Fuel Cells: Alternative Electrochemical Energy Conversion Technologies for the Future

One of the main challenges of the 21st century is developing renewable energy sources. Currently, most of the world's energy originates from fossil fuels and nuclear sources. However, fossil fuels are limited and are one of the biggest causes of CO_2 and other greenhouse gas (GHG) emissions. Indeed, burning fossil fuels is responsible for the majority of global anthropogenic GHG emissions. According to the 2018 Global Carbon Budget [1], the total amount of CO_2 released from fossil fuel consumption was 9.4 ± 0.5 GtC yr^{-1} in the period 2008-2017 and the global atmospheric CO_2 concentration reached an average of 405.0 ± 0.1 ppm. Meanwhile, 350 ppm of atmospheric CO_2 is the consensus limit whereby a 1.5 °C increase in global temperature above pre-industrial levels is achieved and catastrophic climate change can be avoided. However, novel carbon neutral or carbon negative energy strategies are necessary to reach this goal [2,3].

According to a study conducted by the European Environmental Agency (EEA) in 2009, road transport accounts for 17% of GHG emissions, as well as other air pollutants such as carbon monoxide (CO) and nitrogen oxides (NO_x) [4]. A survey conducted by the U.S. Department of Energy (USDE) reported that 15% of the total fuel energy is consumed by automobiles, leading to adverse environmental impacts such as climate change and an alarming increase in pollution [5].

It is estimated that the numbers of vehicles in the world will rise to 3 billion by 2050. Thus, research on clean energy conversion technologies which are not reliant on fossil fuels and are environmentally friendly is essential [3,6].

The electric vehicle (EV) has gained much attention in the last ten years and is considered one way of mitigating climate change caused by GHG. Although EV were introduced in the 1800s, they were not popular until the present decade. As per The Electric Vehicle World Sales Database, EV sales reached over 3.2 million in total as of 2020. This increased popularity of EV can be attributed to the advancement of energy storage devices such as lithium-ion (Li-ion) batteries [7]. Lightweight, high specific power and high energy density make Li-ion batteries promising electrochemical energy storage devices. However, they have technological limitations such as limited operational range [6], long charging duration [7], and high production cost [5] that need to be overcome.

Alternatively, fuel cells (FC) are viewed as one of the most potentially clean energy conversion devices due to low emissions, high efficiency, and smaller size [8]. Moreover, when using liquid fuels they can take advantage of existing infrastructure already in use for petroleum vehicles and power generation with minimal adaptation. They can be constructed in a wide range of sizes to generate energy from microwatts to megawatts, which suits a broad range of uses, from automobiles to localized power generations for small cities [9]. On other hand, fuel cells use externally supplied reactants which are oxidized to supply a current and can function continuously as long as fuel is available; however, batteries require charging which is often time consuming and inconvenient [10]. Most FC vehicles (FCV) employ a FC with a proton exchange membrane (PEM). They have a power output up to 100 kW or more, providing a driving range of 400-500 kilometres. However, use of expensive Pt based catalysts which drives the electrochemical reaction in the FC significantly increases the overall cost of the system. This can be curbed in several ways: (1) by increasing the number of active Pt sites and hence boosting the utilisation of Pt, (2) by replacing it with other non-precious metals, (3) Using organic compounds such as ionic liquids and conducting polymer as effective promoters [11–13]. However, the cost of FC systems and requirement of high purity fuel is still a crucial challenge towards their commercialization. Contrarily there are no moving parts involved in the system which saves the maintenance time and cost. Additionally, unlike batteries, FC are not prone to corrosion and have a longer life span [14]. Further developments and research are needed to lower the cost of FCV [15].

1.1.1 History of fuel cell

Welsh physicist William Robert Grove, or a German Chemist Christian Friedrich Schönbein, provided the first experimental evidence for the FC around the late 1830's [16]. It is argued that Grove discovered the electrochemical process behind the hydrogen FC at that time [17]. Later, the alkaline FC (AFC) was developed in 1932, named after the engineer Francis Thomas Bacon, descendant of the famous philosopher Sir Francis Bacon. One of the earliest uses of FC was by the National Aeronautics and Space Administration (NASA) in the mid-1960s as a clean energy source during the Gemini space mission. FC were further modified and commercialized by General Electric (GE) company in 1955 [18].

1.1.2 What is a fuel cell?

A FC is similar to a battery, which converts chemical energy into electrical energy. However, it does not require charging, unlike batteries, as long as the fuel and oxidant are constantly supplied [19]. There are many sorts of FC depending upon the electrolyte employed, the fuel used, and operating temperature range, but all of them consist of a cathode, an anode, and an electrolyte.

Since this process does not follow Carnot's thermodynamics it has higher theoretical efficiencies than a system driven by combustion [19–21]. A schematic representation of a direct alcohol FC (DAFC) is shown below.

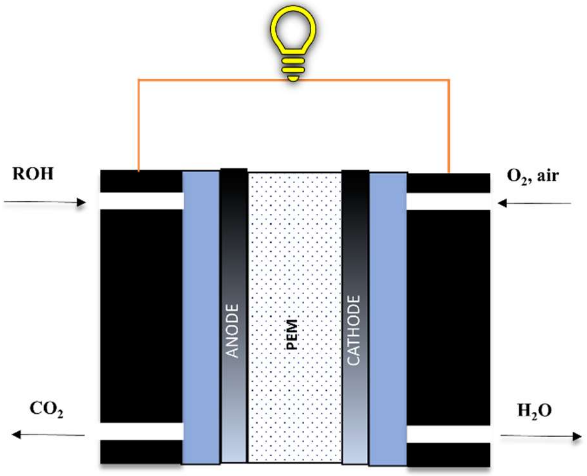

Figure 1.1: A schematic diagram of a direct alcohol fuel cell (DAFC), where the electrochemical oxidation of fuel occurs at the anode, and the oxidant is reduced at the cathode

1.1.3 Types of fuel cell

Depending on the electrolyte employed, FC are divided into alcohol fuel cell (AFC), polymer electrolyte membrane FC (PEMFC), phosphoric acid FC (PAFC), solid oxide FC (SOFC) and molten carbonate FC (MCFC) [22,23]. The main features of each type of FC are summarized in Table 1.1.

Type	AFC	PEMFC	PAFC	SOFC	MCFC
Operating Temperature (°C)	100-200	60-140	150-200	500-1200	600-700
Fuel	H_2	H_2	H_2	CH_X, CO, H_2	CH_X, CO, H_2
Catalyst	Platinum	Platinum	Platinum	Nickel	Perovskites

Table 1.1: Different types of fuel cells and their operating conditions.

1.1.4 Proton exchange membrane fuel cell

PEMFC, also known as a polymer electrolyte membrane FC, are the most promising FC type for portable applications due to their quick start-up, flexibility in any alignment, non-corrosiveness and low working temperature [16]. Hydrogen is considered the preferred fuel for PEMFC, but hydrogen is highly flammable, expensive, and presently dependent on fossil fuel for its production as well as challenging to store and transport.

Therefore, short-chain alcohols such as ethanol and methanol, and FA, which have a broad liquid range and are more easily stored/transported, are considered as alternatives. In this sense, DAFC, or particularly direct methanol fuel cells (DMFC) have emerged as an excellent alternative power source due to the ease of handling and storage of methanol in comparison to hydrogen fuel [24]. Furthermore, DMFC is an appealing power source for portable applications. A DMFC called Emily manufactured by the Smart fuel cell company (SFC) is used by several armed forces around the world which produces a power output of 100 W. It has become a popular alternative in the telecommunications sector as a backup power source in remote locations where electricity is unavailable [25,26].

The optimum operating temperature of a PEMFC is between 60-80 °C, which makes it more feasible for many applications. However, the high costs and breakdown of membrane materials are still bottlenecks to their commercialization [27]. The electrolyte membranes are placed between the two catalyst layers deposited on the anode and cathode and is used to separate the chemical reactions occurring on either electrode. A schematic diagram of the 9-anode proton exchange membrane cell, used for anode catalyst sceening, is shown in Figure 1.2 [28].

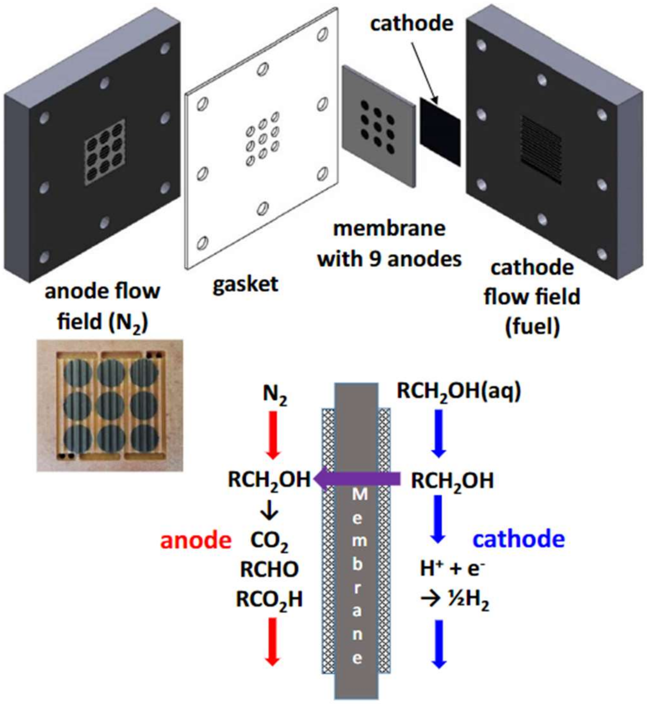

Figure 1.2: A schematic diagram of the 9-anode proton exchange membrane cell

The electrolyte membrane, made up of ionomers, allows the flow of protons but is impermeable to electrons. These membranes should possess certain essential functionalities such as prolonged chemical and thermal stability, high proton or ionic conductivity; low fuel crossover; and low cost [27,29]. The capability of a membrane to absorb and supply water is also vital to its function as low water content leads to an increase in ionic resistance of the cell, while too much hydration results in swelling of the membrane.

Perfluorinated sulfonic acid electrolyte membranes, particularly Nafion® [30], are normally used due to their excellent chemical stability and high proton conductivity. However, they have certain drawbacks, such as high production cost and high permeability, leading to swelling problems, crossover, and loss of fuel. Nafion membranes are thermally stable up to 100 °C, after which they become dehydrated, causing a drop in proton conductivity. Apart from Nafion, many other electrolyte membrane materials have been investigated; for instance, polyvinyl alcohol (PVA), polybenzimidazole (PBI) and sulfonated polyether ether ketone (SPEEK) [31,32].

1.2 Ionic Liquids

Paul Walden, in 1914, likely reported the first ionic liquid (IL), ethyl ammonium nitrate [33] a class of organic salt having a melting point lower than 100 °C and negligible vapour pressures [34]; some examples of the various cationic and anionic IL components are shown in Figure 1.3. IL are also characterized by their excellent thermal and electrochemical stability [35–37]; however, owing to their high viscosities and hygroscopic nature, they can be challenging to manipulate in the laboratory. IL that are liquid at room temperature are sometimes called ‘room temperature ionic liquids’ (RTIL) [38], while generally they are also classified as protic, aprotic, and zwitterionic, based on their composition.

In addition, IL possesses a weakly coordinating ionic character due to having a massive singly-charged organic cation that can be paired with an inorganic anion [39]. As their physical and chemical properties are dependent on their structure, they are also referred to as "designer liquids" for use in specialized applications. A range of IL have been synthesized by changing the cations and anions; these have been employed as a medium for chemical synthesis where traditional solvents are not applicable [40,41]. Due to their unique physicochemical properties, IL have opened up limitless applications in lubricants and seals [34,41–43].

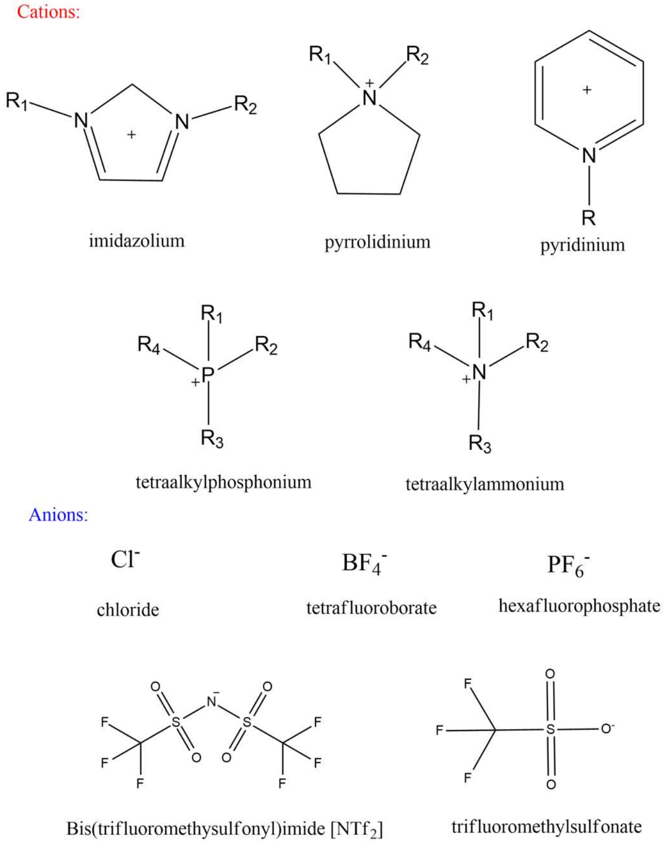

Figure 1.3: Commonly used cation and anion components of IL

IL act as effective media for chemical reactions as well as reagents, catalysts, electrolytes, and dispersion media for nanoparticles (NPs) and colloids [41,44]. Among these applications, the use of IL in the electrodeposition of metals and semiconductors is highly impressive. Electroplating in a water bath is not viable for water-sensitive metals such as aluminum; however, it becomes possible in IL [45], and has been explored in the literature on several occasions, and is likely highly commercializable [46,47].

1.3 Ionic liquid applications

Owing to their unique properties elucidated above, IL have been employed in a variety of applications. They have shown the capability to modify carbon material surfaces to improve their stability and introduce additional ample binding sites for metal NPs [48]. IL-modified carbon materials exhibit high charge transfer activity and high electronic conductivity [49,50].

IL are being investigated as potential electrolytes for fuel cell reactions due to their excellent stability and better performance than inorganic acidic/basic electrolytes [51]. This performance can be attributed to the high solubility of reactant gases and good mass transport properties. IL enables one to carry out reactions even at high temperature and over a wide potential range, making them a promising electrolyte for lithium-ion and solar batteries [34,52,53].

Recently IL have been employed in the synthesis of metal NPs, yielding NPs which are monodisperse with sizes < 20 nm in diameter [54]; Moreover, IL have been used to control the final NP morphologies which has been used to elicit enhanced catalytic properties [40]. Inhwan Do et al. [55] synthesized Pt NPs on various carbon supports such as graphite nanoplatelets (GNP), single-walled carbon nanotubes (SWCNT), multi-walled carbon nanotubes (MWCNT), and carbon black (CB) using two RTIL, butyl-3-methylimidazolium hexafluorophosphate ($bmimPF_6$) and 1-butyl-3-methylimidazolium acetate ($bmimCH_3CO_2$), yielding nanoparticles with a narrow size distribution. In the absence of RTIL, the average particle size was 3.74 nm which was reduced to 2.0 nm when one was present. Do et al. further revealed that the size of metal NPs could be controlled by varying the RTIL concentration during the process of NP formation [55].

The synthesis of metal-NPs in IL is generally carried out by chemical or photochemical reduction, microwave irradiation, or electroreduction. Traditional nanoparticle synthetic methods often employ a capping agent; for example, alcohols, amines, thiols, and organic acids [38,44]. Capping agents act as a stabilizer, preventing uncontrolled growth, morphological changes, and aggregation of NPs [41]. When used as a catalyst, NP stability is crucial for retaining catalytic activity [54,56]. Stabilization of metal NPs arises through steric or electrostatic forces; however, IL act through a combination of both owing to their supramolecular nature often referred to as 'electrosteric' stabilization [40,57], the mechanism of which is not fully understood. Seemingly, NP aggregation is also not an issue as it produces highly mono-dispersed NPs that are stable for months when stored under inert conditions [56,58,59]; i.e., in the absence of O_2.

Lately, IL have been proposed as catalysts in the electro-reduction of N_2 to ammonia [60]. Ammonia is an essential commodity for use as fertilizers in agriculture as well as in manufacturing and refrigeration. Presently, it is produced by the Haber-Bosch process which is not environmentally friendly due to the significant emission of CO_2 [61–63]. Alternatively, electrochemically synthesized ammonia offers a zero-carbon emission pathway. The current drawback with this reaction is the use of a sacrificial proton source, typically ethanol. However, Suryanto *et al*. [60] employed a phosphonium IL incorporating the trihexyltetradecylphosphonium $[P_{6,6,6,14}]^+$ cation as a proton shuttle in the electrochemical N_2 reduction reaction (NRR) to overcome this drawback and found it can stably undergo repeated cycles of deprotonation-reprotonation, with enhanced ionic conductivity.

1.4 Organic ionic plastic crystals (OIPC)

Ikeda [64] and Nakamura [65] reported the early class of organic ionic plastic crystals (OIPC). OIPC is a class of IL that have gained popularity due to their state-of-the-art physical properties and applications in lithium and sodium-ion batteries, fuel cells, and solar cells [66] They have the same physicochemical properties as IL except that they are solid at room temperature and have multiple solid-solid phase transitions below their melting point. [67,68]. Plastic crystals are polycrystalline materials with long-range crystalline lattices, possessing local orientation and/or rotational disorder. The first solid-solid phase transition (Phase 1) is considered the uttermost plastic and conductive phase [69] and exists just below the melting point. As suggested by Timmermans, OIPC should exhibit a small entropy of fusion $\left(\Delta S_{fusion} < 20\,JK^{-1}mol^{-1}\right)$, permitting them the properties of plasticity [66,67,70]. As a consequence of this complex phase behaviour, the ion transport properties of OIPC are dependant on temperature [71]. It can be considered that OIPC exist in a state of matter intermediate between solid and liquid, also known as mesophases [72]. Several factors could be responsible for its conductive nature; however, vacancies in the crystal structure and conformational disorder of the individual ions likely contribute [73]. Forsyth's group has studied the ion conduction mechanisms in OIPC using solid-state NMR as well as magnetic resonance imaging (MRI) [74,75]. This work highlighted the polycrystalline nature of OIPC and that, aside from proton hopping in protic IL, ion conduction likely occurs along grain boundaries. In the case of protic OIPC, proton hopping likely occurs through a Grotthuss mechanism similar to the H-bond breaking and forming in liquid water, however, in the solid phase. An example of a phosphonium cation based OIPC is shown below in Figure 1.4

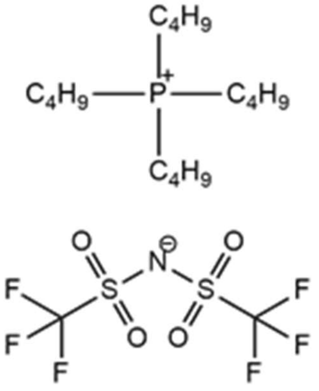

Figure 1.4: Structure of tetrabutylphosphonium bis(trifluoromethylsulfonyl)imide ($P_{4444}NTf_2$) organic ionic plastic crystal (OIPC).

Owing to their high proton conductivity in comparison to polymers, protic OIPC can be substituted in place of traditional polymer-based electrolytes (e.g. Nafion), exploiting their inherent hydrophobicity in anhydrous cases where Nafion is unsuitable [76]. Luo. *et al.* [72] developed a fuel cell using a 1,2,4-Triazolium perfluorobutanesulfonate [TAZm][PFBS] as the proton-conducting membrane and were successful; however, long-term stability and durability still need to be explored. Use of OIPC, similar to other solid-state electrolytes, eliminates the complication of electrolyte leakage.

1.5 Scope of the Thesis

The scientific community has put much effort into developing renewable energy conversion technology such as FC. Even though this technology is not new, interest in FC has slipped due to fluctuating support from industry and government owing to the cheap cost of fossil fuels. However, due to adverse environmental impacts associated with conventional energy sources such as climate change, a great deal of research towards the widespread commercialization of FC is underway. Within the above introductory chapter an overview of the need for alternative clean energy conversion technologies and its history has been developed. Followed by adecription of the state-of-the-art applications of IL and OIPC in the field of electrochemistry.

Chapter 2 focuses on modifying a commercial Pt/C catalyst for FA (FA) oxidation with an OIPC for enhanced activity and stability. An enhancement of up to 2.5 times was seen after OIPC modification. Followed by characterization of OIPC itself and the catalyst. It indicates the vital role of hydrophobicity of the OIPC layer on the catalyst surface and the thermal properties of both are discussed in detail.

In Chapter 3, a variety of hydrophobic IL were synthesized with varying alkyl chain lengths from 4 to 8 carbons for the fourth arm, while the other three remained the same. Methanol was chosen as the desired fuel out of ease of handling and storage. All the catalysts were characterized by cyclic voltammetry (CV) for catalytic activity followed by durability testing in a 9 anode PEMFC flow cell. Thermogravimetric analysis (TGA) and differential scanning calorimetry (DSC) were employed to investigate the thermal behaviour of as-prepared IL/OIPC and catalyst materials. This chapter reveals how the cationic chain length of one R group of the IL influences the catalytic activity of the catalyst.

Finally, Chapter 4 summarises all the preceding work in the SC-OIPC/SCILL system. Since a small amount of IL is used, it results in a considerable cost reduction for catalyst modification in that a similar performance can be achieved, however, with a much lower Pt loading. Since a very thin layer of the OIPC is formed, the viscosity of IL does not affect the course of the reaction, and reduced mass transfer does not create a problem. It was also highlighted that the catalytic behaviour could be manipulated by the rational design of IL structures. All these works imply that IL modification is a powerful method to improve the catalytic performance of various oxidation reactions. However, more studies are still needed to better understand this enhancement at a molecular level towards its practical application.

1.6 References

[1] C. Quéré, R. Andrew, P. Friedlingstein, S. Sitch, J. Hauck, J. Pongratz, P. Pickers, J. Ivar Korsbakken, G. Peters, J. Canadell, A. Arneth, V. Arora, L. Barbero, A. Bastos, L. Bopp, P. Ciais, L. Chini, P. Ciais, S. Doney, T. Gkritzalis, D. Goll, I. Harris, V. Haverd, F. Hoffman, M. Hoppema, R. Houghton, G. Hurtt, T. Ilyina, A. Jain, T. Johannessen, C. Jones, E. Kato, R. Keeling, K. Klein Goldewijk, P. Landschützer, N. Lefèvre, S. Lienert, Z. Liu, D. Lombardozzi, N. Metzl, D. Munro, J. Nabel, S.I. Nakaoka, C. Neill, A. Olsen, T. Ono, P. Patra, A. Peregon, W. Peters, P. Peylin, B. Pfeil, D. Pierrot, B. Poulter, G. Rehder, L. Resplandy, E. Robertson, M. Rocher, C. Rödenbeck, U. Schuster, I. Skjelvan, R. Séférian, I. Skjelvan, T. Steinhoff, A. Sutton, P. Tans, H. Tian, B. Tilbrook, F. Tubiello, I. van der Laan-Luijkx, G. van der Werf, N. Viovy, A. Walker, A. Wiltshire, R. Wright, S. Zaehle, B. Zheng, Global Carbon Budget 2018, Earth System Science Data. 10 (2018) 2141–2194. https://doi.org/10.5194/essd-10-2141-2018.

[2] R. Quadrelli, S. Peterson, The Energy-Climate Challenge: Recent Trends in CO_2 Emissions from Fuel Combustion, Energy Policy. 35 (2007) 5938–5952. https://doi.org/10.1016/j.enpol.2007.07.001.

[3] M.S. Dresselhaus, I.L. Thomas, Alternative Energy Technologies, Nature. 414 (2001) 332–337. https://www.nature.com/articles/35104599.

[4] A. Ziegler, Individual Characteristics and Stated Preferences for Alternative Energy Sources And Propulsion Technologies in Vehicles: A Discrete Choice Analysis for Germany, Transportation Research Part A: Policy and Practice. 46 (2012) 1372–1385. https://doi.org/10.1016/j.tra.2012.05.016.

[5] S.F. Tie, C.W. Tan, A Review of Energy Sources and Energy Management System in Electric Vehicles, Renewable and Sustainable Energy Reviews. 20 (2013) 82–102. https://doi.org/10.1016/j.rser.2012.11.077.

[6] R.T. Doucette, M.D. McCulloch, Modeling the Prospects of Plug-in Hybrid Electric Vehicles to Reduce CO_2 Emissions, Applied Energy. 88 (2011) 2315–2323. https://doi.org/10.1016/j.apenergy.2011.01.045.

[7] Z.P. Cano, D. Banham, S. Ye, A. Hintennach, J. Lu, M. Fowler, Z. Chen, Batteries and Fuel Cells for Emerging Electric Vehicle Markets, Nature Energy. 3 (2018) 279–289. https://doi.org/10.1038/s41560-018-0108-1.

[8] D. Akinyele, E. Olabode, A. Amole, Review of Fuel Cell Technologies and Applications for Sustainable Microgrid Systems, Inventions. 5 (2020) 1–35. https://doi.org/10.3390/inventions5030042.

[9] S. Song, P. Tsiakaras, Recent Progress in Direct Ethanol Proton Exchange Membrane Fuel Cells (DE-Pemfcs), Applied Catalysis B: Environmental. 63 (2006) 187–193. https://doi.org/10.1016/j.apcatb.2005.09.018.

[10] A.G. Olabi, T. Wilberforce, M.A. Abdelkareem, Fuel Cell Application in the Automotive Industry and Future Perspective, Energy. 214 (2021). https://doi.org/10.1016/j.energy.2020.118955.

[11] A. Alaswad, A. Omran, J.R. Sodre, T. Wilberforce, G. Pignatelli, M. Dassisti, A. Baroutaji, A.G. Olabi, Technical and Commercial Challenges of Proton-Exchange Membrane (PEM) Fuel Cells, Energies. 14 (2021). https://doi.org/10.3390/en14010144.

[12] R.B. Moghaddam, P.G. Pickup, Mechanistic Studies of Formic Acid Oxidation at Polycarbazole Supported Pt Nanoparticles, Electrochimica Acta. 111 (2013) 823–829. https://doi.org/10.1016/j.electacta.2013.08.098.

[13] M. George, G.R. Zhang, N. Schmitt, K. Brunnengräber, D.J.S. Sandbeck, K.J.J. Mayrhofer, S. Cherevko, B.J.M. Etzold, Effect of Ionic Liquid Modification on the ORR Performance and Degradation Mechanism of Trimetallic PtNiMo/C Catalysts, ACS Catalysis. 9 (2019) 8682–8692. https://doi.org/10.1021/acscatal.9b01772.

[14] I.S. Sorlei, N. Bizon, P. Thounthong, M. Varlam, E. Carcadea, M. Culcer, M. Iliescu, M. Raceanu, Fuel Cell Electric Vehicles—A Brief Review of Current Topologies and Energy Management Strategies, Energies. 14 (2021). https://doi.org/10.3390/en14010252.

[15] A. Ajanovic, R. Haas, Economic and Environmental Prospects for Battery Electric- and Fuel Cell Vehicles: A Review, Fuel Cells. 19 (2019) 515–529. https://doi.org/10.1002/fuce.201800171.

[16] H.R. Corti, E.R. Gonzalez, eds., Direct Alcohol Fuel Cells, Springer Netherlands, Dordrecht, 2014. https://doi.org/10.1007/978-94-007-7708-8.

[17] J.M. Andújar, F. Segura, Fuel cells: History and Updating. A Walk Along Two Centuries, Renewable and Sustainable Energy Reviews. 13 (2009) 2309–2322. https://doi.org/10.1016/j.rser.2009.03.015.

[18] K. v Kordesch, G.R. Simader, Environmental Impact of Fuel Cell Technology, 1995. https://pubs.acs.org/sharingguidelines.

[19] R.N. Singh, Madhu, R. Awasthi, Alcohol Fuel Cells, in: New and Future Developments in Catalysis: Batteries, Hydrogen Storage and Fuel Cells, Elsevier B.V., 2013: pp. 453–478. https://doi.org/10.1016/B978-0-444-53880-2.00021-1.

[20] T. dos S. Almeida, A.R. de Andrade, New Trends in Direct Ethanol Fuel Cells, in: New and Future Developments in Catalysis: Batteries, Hydrogen Storage and Fuel Cells, Elsevier B.V., 2013: pp. 429–452. https://doi.org/10.1016/B978-0-444-53880-2.00020-X.

[21] K. Kakaei, A. Ehsani, Direct Alcohol Fuel Cells Graphene Surfaces 7.2.1 Introduction Development of Direct Alcohol Fuel Cells Components, 2019. https://doi.org/10.1016/B978-0-12-814523-4.00001-0.

[22] F. Gao, M. Kabalo, M.S. Rylko, B. Blunier, A. Miraoui, Fuel Cell System, 2013. https://doi.org/10.1007/978-1-4471-5104-3_6.

[23] J. Melorose, R. Perroy, S. Careas, Fuel Cell Technology Reaching Towards Commercialization, Statewide Agricultural Land Use Baseline 2015. 1 (2015) 1–306. https://doi.org/https://doi.org/10.1007/1-84628-207-1.

[24] E.H. Yu, K. Scott, Development of Direct Methanol Alkaline Fuel Cells Using Anion Exchange Membranes, Journal of Power Sources. 137 (2004) 248–256. https://doi.org/10.1016/j.jpowsour.2004.06.004.

[25] M.S. Alias, S.K. Kamarudin, A.M. Zainoodin, M.S. Masdar, Active Direct Methanol Fuel Cell: An Overview, International Journal of Hydrogen Energy. 45 (2020) 19620–19641. https://doi.org/10.1016/j.ijhydene.2020.04.202.

[26] S.K. Kamarudin, F. Achmad, W.R.W. Daud, Overview on the Application of Direct Methanol Fuel Cell (DMFC) For Portable Electronic Devices, International Journal of Hydrogen Energy. 34 (2009) 6902–6916. https://doi.org/10.1016/j.ijhydene.2009.06.013.

[27] S. Sharma, B.G. Pollet, Support Materials for PEMFC And DMFC Electrocatalysts - A Review, Journal of Power Sources. 208 (2012) 96–119. https://doi.org/10.1016/j.jpowsour.2012.02.011.

[28] T.M. Brueckner, P.G. Pickup, Kinetics and Stoichiometry of Methanol and Ethanol Oxidation in Multi-Anode Proton Exchange Membrane Cells, Journal of The Electrochemical Society. 164 (2017) F1172–F1178. https://doi.org/10.1149/2.1181712jes.

[29] D.E. Curtin, R.D. Lousenberg, T.J. Henry, P.C. Tangeman, M.E. Tisack, Advanced Materials for Improved PEMFC Performance and Life, Journal of Power Sources. 131 (2004) 41–48. https://doi.org/10.1016/j.jpowsour.2004.01.023.

[30] D.J. Connolly, W. Frank, D. Nemours, United States Patent Office: Fluorocarbon Vinyl Ether Polymers, (1966).

[31] S. Song, P. Tsiakaras, Recent progress in Direct Ethanol Proton Exchange Membrane Fuel Cells (DE-PEMFCs), Applied Catalysis B: Environmental. 63 (2006) 187–193. https://doi.org/10.1016/j.apcatb.2005.09.018.

[32] F. Maillard, N. Job, M. Chatenet, Basics of PEMFC Including the Use of Carbon-Supported Nanoparticles, in: New and Future Developments in Catalysis: Catalysis by Nanoparticles, Elsevier Inc., 2013: pp. 401–423. https://doi.org/10.1016/B978-0-444-53874-1.00018-4.

[33] Z. Lei, B. Chen, Y.M. Koo, D.R. Macfarlane, Introduction: Ionic Liquids, Chemical Reviews. 117 (2017) 6633–6635. https://doi.org/10.1021/acs.chemrev.7b00246.

[34] M. Watanabe, M.L. Thomas, S. Zhang, K. Ueno, T. Yasuda, K. Dokko, Application of Ionic Liquids to Energy Storage and Conversion Materials and Devices, Chemical Reviews. 117 (2017) 7190–7239. https://doi.org/10.1021/acs.chemrev.6b00504.

[35] K.J. Fraser, D.R. MacFarlane, Phosphonium-Based Ionic Liquids: An Overview, Australian Journal of Chemistry. 62 (2009) 309–321. https://doi.org/10.1071/CH08558.

[36] T.J. Stockmann, P.D. Boyle, Z. Ding, Preparation and Crystal Structure of Tetraoctylphosphonium Tetrakis(Pentafluorophenyl)Borate Ionic Liquid for Electrochemistry at its Interface with Water, Catalysis Today. 295 (2017) 89–94. https://doi.org/10.1016/j.cattod.2017.05.030.

[37] R. Moshrefi, A. Suryawanshi, T.J. Stockmann, Electrochemically Controlled Au Nanoparticle Nucleation at a Micro Liquid/Liquid Interface Using Ferrocene as Reducing Agent, Electrochemistry Communications. 122 (2021) 106894. https://doi.org/10.1016/j.elecom.2020.106894.

[38] Y. Cao, J. Wu, J. Zhang, H. Li, Y. Zhang, J. He, Room Temperature Ionic Liquids (RTILs): A New and Versatile Platform for Cellulose Processing and Derivatization, Chemical Engineering Journal. 147 (2009) 13–21. https://doi.org/10.1016/j.cej.2008.11.011.

[39] K. Dong, X. Liu, H. Dong, X. Zhang, S. Zhang, Multiscale Studies on Ionic Liquids, Chemical Reviews. 117 (2017) 6636–6695. https://doi.org/10.1021/acs.chemrev.6b00776.

[40] Z. He, P. Alexandridis, Nanoparticles in Ionic Liquids: Interactions and Organization, Physical Chemistry Chemical Physics. 17 (2015) 18238–18261. https://doi.org/10.1039/c5cp01620g.

[41] S.K. Singh, A.W. Savoy, Ionic Liquids Synthesis and Applications: An Overview, Journal of Molecular Liquids. 297 (2020) 112038. https://doi.org/10.1016/j.molliq.2019.112038.

[42] A. Balducci, Ionic Liquids in Lithium-Ion Batteries, Topics in Current Chemistry. 375 (2017). https://doi.org/10.1007/s41061-017-0109-8.

[43] T. Welton, Ionic Liquids: A Brief History, Biophysical Reviews. 10 (2018) 691–706. https://doi.org/10.1007/s12551-018-0419-2.

[44] J.P. Hallett, T. Welton, Room-Temperature Ionic Liquids: Solvents for Synthesis and Catalysis. 2, Chemical Reviews. 111 (2011) 3508–3576. https://doi.org/10.1021/cr1003248.

[45] M. Armand, F. Endres, D.R. MacFarlane, H. Ohno, B. Scrosati, Ionic-Liquid Materials for the Electrochemical Challenges of the Future, Nature Materials. 8 (2009) 621–629. https://doi.org/10.1038/nmat2448.

[46] S. Zein El Abedin, E.M. Moustafa, R. Hempelmann, H. Natter, F. Endres, Electrodeposition of Nano and Macrocrystalline Aluminium in Three Different Air and Water Stable Ionic Liquids, ChemPhysChem. 7 (2006) 1535–1543. https://doi.org/10.1002/cphc.200600095.

[47] S.Z. el Abedin, Coating of Mild Steel by Aluminium in the Ionic Liquid [EMIm]Tf2N and its Corrosion Performance, Zeitschrift Fur Physikalische Chemie. 220 (2006) 1293–1308. https://doi.org/10.1524/zpch.2006.220.10.1293.

[48] G.R. Zhang, B.J.M. Etzold, Ionic liquids in electrocatalysis, Journal of Energy Chemistry. 25 (2016) 199–207. https://doi.org/10.1016/j.jechem.2016.01.007.

[49] Q. Zhang, J. Zhang, B. Liu, L. Zhang, L. Dong, E. Li, H. Zhang, L. Xia, Thermally Responsive Reduced Graphene Oxide with Designable Secondary Functionality, Chemical Communications. 53 (2017) 6367–6370. https://doi.org/10.1039/c7cc03230g.

[50] L.-H. Liu, C.-Q. Duan, Z.-N. Gao, Electrochemical Behavior and Electrochemical Determination of Tiamulin Fumarate at an Ionic Liquid Modified Carbon Paste Electrode, Croat. Chem. Acta. 83 (2010) 409–414.

[51] A. Ray, B. Saruhan, Application of Ionic Liquids for Batteries and Supercapacitors, Materials. 14 (2021). https://doi.org/10.3390/ma14112942.

[52] A. Balducci, Ionic Liquids in Lithium-Ion Batteries, Topics in Current Chemistry. 375 (2017). https://doi.org/10.1007/s41061-017-0109-8.

[53] Y.S. Ye, J. Rick, B.J. Hwang, Ionic Liquid Polymer Electrolytes, Journal of Materials Chemistry A. 1 (2013) 2719–2743. https://doi.org/10.1039/c2ta00126h.

[54] A. Banerjee, R.W.J. Scott, Optimization of Transition Metal Nanoparticle-Phosphonium Ionic Liquid Composite Catalytic Systems for Deep Hydrogenation and Hydrodeoxygenation Reactions, Green Chemistry. 17 (2015) 1597–1604. https://doi.org/10.1039/c4gc01716a.

[55] I. Do, L.T. Drzal, Ionic Liquid-Assisted Synthesis of Pt Nanoparticles onto Exfoliated Graphite Nanoplatelets for Fuel Cells, ACS Applied Materials and Interfaces. 6 (2014) 12126–12136. https://doi.org/10.1021/am5012832.

[56] U. Kernchen, B. Etzold, W. Korth, A. Jess, Solid Catalyst Ionic Liquid Layer (SCILL) - A New Concept to Improve Selectivity Illustrated by Hydrogenation of Cyclooctadiene, Chemical Engineering and Technology. 30 (2007) 985–994. https://doi.org/10.1002/ceat.200700050.

[57] O. Bartlewicz, I. Dąbek, A. Szymańska, H. Maciejewski, Heterogeneous Catalysis With The Participation of Ionic Liquids, Catalysts. 10 (2020) 1–16. https://doi.org/10.3390/catal10111227.

[58] J. Xu, B. Liu, W. Wu, C. Qian, Q. Wu, X. Lin, W.A. Chem, I. Ed, Basic Ionic Liquid as Catalysis and Reaction Medium : A Novel and Green Protocol for the Markovnikov Addition of N -Heterocycles to Vinyl Esters , Using a Task-Specific Ionic Liquid , [bmIm] OH Recei V ed January 16 , 2006 A basic ionic liquid , 1-methy, The Journal of Organic Chemistry. 71 (2006) 3991–3993. https://doi.org/doi/10.1021/jo0600914.

[59] Y. Zhang, B. Zhen, H. Li, Y. Feng, Basic Ionic Liquid as Catalyst and Surfactant: Green Synthesis of Quinazolinone in Aqueous Media, RSC Advances. 8 (2018) 36769–36774. https://doi.org/10.1039/C8RA06378H.

[60] B.H.R. Suryanto, K. Matuszek, J. Choi, R.Y. Hodgetts, H.-L. Du, J.M. Bakker, C.S.M. Kang, P. v Cherepanov, A.N. Simonov, D.R. Macfarlane, Nitrogen Reduction to Ammonia at High Efficiency and Rates Based on a Phosphonium Proton Shuttle, Science. 372 (2021) 1187–1191. http://science.sciencemag.org/.

[61] J. Deng, J.A. Iñiguez, C. Liu, Electrocatalytic Nitrogen Reduction at Low Temperature, Joule. 2 (2018) 846–856. https://doi.org/10.1016/j.joule.2018.04.014.

[62] S. Vaclav, Detonator of the Population Explosion, Nature. 400 (1999).

[63] J. Chatt, J.R. Dilworth, R.L. Richards, Recent Advances in the Chemistry of Nitrogen Fixation, 1978. https://pubs.acs.org/sharingguidelines.

[64] M. Tansho, D. Nakamura, R. Ikeda, Thermodynamically Metastable Plastic Phase revealed in Methylammonium Bromide Crystals, 1991.

[65] ishida Hiroyuki, ikeda Ryuichi, 1H NMR Studies on the Motion of Cations in the Three Solid Phases of Methylammonium Perchlorate Including Cationic Self-Diffusion in Its Highest-Temperature Solid Phase, Bulletin of the Chemical Society of Japan. 60 (1987) 467–474.

[66] H. Zhu, D.R. MacFarlane, J.M. Pringle, M. Forsyth, Organic Ionic Plastic Crystals as Solid-State Electrolytes, Trends in Chemistry. 1 (2019) 126–140. https://doi.org/10.1016/j.trechm.2019.01.002.

[67] H. Zhu, X. Wang, R. Vijayaraghava, Y. Zhou, D.R. Macfarlane, M. Forsyth, Structure and Ion Dynamics in Imidazolium-Based Protic Organic Ionic Plastic Crystals, Journal of

Physical Chemistry Letters. 9 (2018) 3904–3909. https://doi.org/10.1021/acs.jpclett.8b01500.

[68] J.M. Pringle, P.C. Howlett, D.R. MacFarlane, M. Forsyth, Organic Ionic Plastic Crystals: Recent Advances, Journal of Materials Chemistry. 20 (2010) 2056–2062. https://doi.org/10.1039/b920406g.

[69] L. Jin, P.C. Howlett, J.M. Pringle, J. Janikowski, M. Armand, D.R. MacFarlane, M. Forsyth, An Organic Ionic Plastic Crystal Electrolyte for Rate Capability and Stability of Ambient Temperature Lithium Batteries, Energy and Environmental Science. 7 (2014) 3352–3361. https://doi.org/10.1039/c4ee01085j.

[70] J. Timmermans, Plastic Crystals: A Historical Overview, J. Phys. Chem. Solids. 18 (1961) 1–8.

[71] K. Romanenko, J.M. Pringle, L.A. O'Dell, M. Forsyth, New Insights into the Thermal Behaviour of Organic Ionic Plastic Crystals: Magnetic Resonance Imaging of Polycrystalline Morphology Alterations Induced by Solid-Solid Phase Transitions, Physical Chemistry Chemical Physics. 17 (2015) 18991–19000. https://doi.org/10.1039/c5cp03294f.

[72] J. Luo, A.H. Jensen, N.R. Brooks, J. Sniekers, M. Knipper, D. Aili, Q. Li, B. Vanroy, M. Wübbenhorst, F. Yan, L. van Meervelt, Z. Shao, J. Fang, Z.H. Luo, D.E. de Vos, K. Binnemans, J. Fransaer, 1,2,4-Triazolium Perfluorobutanesulfonate as an Archetypal Pure Protic Organic Ionic Plastic Crystal Electrolyte for All-Solid-State Fuel Cells, Energy and Environmental Science. 8 (2015) 1276–1291. https://doi.org/10.1039/c4ee02280g.

[73] J.M. Pringle, Recent Progress in he Development and use of Organic Ionic Plastic Crystal Electrolytes, Physical Chemistry Chemical Physics. 15 (2013) 1339–1351. https://doi.org/10.1039/c2cp43267f.

[74] H. Zhu, X. Wang, R. Vijayaraghava, Y. Zhou, D.R. Macfarlane, M. Forsyth, Structure and Ion Dynamics in Imidazolium-Based Protic Organic Ionic Plastic Crystals, Journal of Physical Chemistry Letters. 9 (2018) 3904–3909. https://doi.org/10.1021/acs.jpclett.8b01500.

[75] K. Romanenko, L. Jin, L.A. Madsen, J.M. Pringle, L.A. Odell, M. Forsyth, Anisotropic MRI Contrast Reveals Enhanced Ionic Transport in Plastic Crystals, Journal of the American Chemical Society. 136 (2014) 15638–15645. https://doi.org/10.1021/ja508290z.

[76] H. Zhu, D.R. MacFarlane, J.M. Pringle, M. Forsyth, Organic Ionic Plastic Crystals as Solid-State Electrolytes, Trends in Chemistry. 1 (2019) 126–140. https://doi.org/10.1016/j.trechm.2019.01.002.

[77] A. Yuda, A. Ashok, A. Kumar, A Comprehensive and Critical Review on Recent Progress in Anode Catalyst for Methanol Oxidation Reaction, Catalysis Reviews - Science and Engineering. (2020). https://doi.org/10.1080/01614940.2020.1802811.

[78] P. Majidi, R.M. Altarawneh, N.D.W. Ryan, P.G. Pickup, Determination of the Efficiency of Methanol Oxidation in a Direct Methanol Fuel Cell, Electrochimica Acta. 199 (2016) 210–217. https://doi.org/10.1016/j.electacta.2016.03.147.

[79] T. Iwasita, Electrocatalysis of Methanol Oxidation, Electrochimica Acta. 47 (2003) 3663–3674. https://doi.org/10.1016/S0013-4686(02)00336-5.

[80] J.M. Ogden, M.M. Steinbugler, T.G. Kreutz, Comparison of Hydrogen, Methanol and Gasoline as Fuels for Fuel Cell Vehicles: Implications for Vehicle Design and Infrastructure Development, Journal of Power Sources. 79 (1999) 143–168. https://doi.org/10.1016/S0378-7753(99)00057-9.

[81] S.S. Pethaiah, K.K. Sadasivuni, A. Jayakumar, D. Ponnamma, C.S. Tiwary, G. Sasikumar, Methanol Electrolysis for Hydrogen Production Using Polymer Electrolyte Membrane: A Mini-Review, Energies. 13 (2020). https://doi.org/10.3390/en13225879.

[82] Z.B. Wang, Y.Y. Chu, A.F. Shao, P.J. Zuo, G.P. Yin, Electrochemical Impedance Studies of Electrooxidation of Methanol and Formic Acid on Pt/C Catalyst in Acid Medium, Journal of Power Sources. 190 (2009) 336–340. https://doi.org/10.1016/j.jpowsour.2009.01.008.

[83] A. Sayadi, P.G. Pickup, Evaluation of Methanol Oxidation Catalysts by Rotating Disc Voltammetry, Electrochimica Acta. 199 (2016) 12–17. https://doi.org/10.1016/j.electacta.2016.03.112.

[84] R.N. Singh, Madhu, R. Awasthi, Alcohol Fuel Cells, in: New and Future Developments in Catalysis: Batteries, Hydrogen Storage and Fuel Cells, Elsevier B.V., 2013: pp. 453–478. https://doi.org/10.1016/B978-0-444-53880-2.00021-1.

[85] S. Wasmus, A. Küver, Methanol Oxidation and Direct Methanol Fuel Cells: A selective Review, Journal of Electroanalytical Chemistry. 461 (1999) 14–31. https://doi.org/10.1016/s0022-0728(98)00197-1.

[86] R.M. Altarawneh, T.M. Brueckner, B. Chen, P.G. Pickup, Product distributions and Efficiencies for Ethanol Oxidation at PtNi Octahedra, Journal of Power Sources. 400 (2018) 369–376. https://doi.org/10.1016/j.jpowsour.2018.08.052.

[87] E.N. el Sawy, P.G. Pickup, Formic Acid Oxidation at Ru@Pt Core-Shell Nanoparticles, Electrocatalysis. 7 (2016) 477–485. https://doi.org/10.1007/s12678-016-0328-8.

[88] X. Ren, Q. Lv, L. Liu, B. Liu, Y. Wang, A. Liu, G. Wu, Current Progress of Pt and Pt-Based Electrocatalysts used for Fuel Cells, Sustainable Energy and Fuels. 4 (2019) 15–30. https://doi.org/10.1039/c9se00460b.

[89] M.K. Debe, Electrocatalyst Approaches and Challenges for Automotive Fuel Cells, Nature. 486 (2012) 43–51. https://doi.org/10.1038/nature11115.

[90] G.R. Zhang, T. Wolker, D.J.S. Sandbeck, M. Munoz, K.J.J. Mayrhofer, S. Cherevko, B.J.M. Etzold, Tuning the Electrocatalytic Performance of Ionic Liquid Modified Pt Catalysts for the Oxygen Reduction Reaction via Cationic Chain Engineering, ACS Catalysis. 8 (2018) 8244–8254. https://doi.org/10.1021/acscatal.8b02018.

[91] X. Zhao, Y. Hu, L. Liang, C. Liu, J. Liao, W. Xing, Ionic Liquid-Mediated Synthesis of "Clean" Palladium Nanoparticles for Formic Acid Electrooxidation, International Journal of Hydrogen Energy. 37 (2012) 51–58. https://doi.org/10.1016/j.ijhydene.2011.09.075.

[92] J. Pitawala, A. Matic, A. Martinelli, P. Jacobsson, V. Koch, F. Croce, Thermal Properties and Ionic Conductivity of Imidazolium Bis(Trifluoromethanesulfonyl)Imide Dicationic Ionic Liquids, Journal of Physical Chemistry B. 113 (2009) 10607–10610. https://doi.org/10.1021/jp904989s.

[93] S. v Dzyuba, R.A. Bartsch, Influence of Structural Variations in 1-Alkyl(aralkyl)-3-Methylimidazolium Hexafluorophosphates and Bis(trifluoromethylsulfonyl)imides on Physical Properties of the Ionic Liquids, ChemPhysChem. 3 (2002) 161–166. https://doi.org/10.1002/1439-7641(20020215)3:2<161::AID-CPHC161>3.0.CO;2-3.

[94] M. Yoshizawa, H. Ohno, Triple Ion-Type Imidazolium Salts: A New Class of Single-Ion Conductive Matrix, Ionics. 8 (2002) 267–271. https://doi.org/DOI:10.1007/BF02376078.

[95] T.J. Stockmann, J. Zhang, A.M. Montgomery, Z. Ding, Electrochemical Assessment of Water|Ionic Liquid Biphasic Systems Towards Cesium Extraction from Nuclear Waste, Analytica Chimica Acta. 821 (2014) 41–47. https://doi.org/10.1016/j.aca.2014.03.012.

[96] A.I. Bhatt, I. May, V.A. Volkovich, M.E. Hetherington, B. Lewin, R.C. Thied, N. Ertok, Group 15 Quaternary Alkyl Bistriflimides: Ionic Liquids with Potential Application in Electropositive Metal Deposition and as Supporting Electrolytes, Journal of the Chemical Society. Dalton Transactions. (2002) 4532–4534. https://doi.org/10.1039/b208968h.

[97] K.J. Fraser, D.R. MacFarlane, Phosphonium-Based Ionic Liquids: An Overview, Australian Journal of Chemistry. 62 (2009) 309–321. https://doi.org/10.1071/CH08558.

[98] U. Domańska, M. Wlazło, M. Karpińska, M. Zawadzki, New Ionic Liquid [$P_{4,4,4,4}$][NTf_2] in Bio-Butanol Extraction on Investigation of Limiting Activity Coefficients, Fluid Phase Equilibria. 475 (2018) 89–94. https://doi.org/10.1016/j.fluid.2018.07.028.

[99] A. Suryawanshi, P.G. Pickup, T.J. Stockmann, Organic Ionic Plastic Crystal Surface Modification of a Commercial Pt/C Catalyst with Enhanced Formic Acid Oxidation or Fuel Cells, Journal of Ionic Liquids. (2021).

[100] K. Huang, T. Song, O. Morales-Collazo, H. Jia, J.F. Brennecke, Enhancing Pt/C Catalysts for the Oxygen Reduction Reaction with Protic Ionic Liquids: The Effect of Anion Structure, Journal of The Electrochemical Society. 164 (2017) F1448–F1459. https://doi.org/10.1149/2.1071713jes.

[101] A.B. Yurtcan, Formic Acid and Methanol Oxidation for Pt/C Catalyst Depending on Rotating Speed, Scan Rate and Concentration, Brilliant Engineering. 1 (2019) 1–4. https://doi.org/10.36937/ben.2020.002.001.

Chapter 2

Organic ionic plastic crystal surface modification of a commercial Pt/C catalyst with enhanced FA oxidation for fuel cells

2.1 Statement of Co-Authorship

This chapter has been submitted under the above title to *Journal of Ionic Liquids*

Authors: Abhishek Suryawanshi, Dr. T. Jane Stockmann, Dr. Peter G. Pickup

Abhishek Suryawanshi is the first author as he performed the bulk of the experimental work and analyzed the data.

2.2 Abstract

Fuel cell technologies will be an integral component of comprehensive green energy strategies aimed towards closing the industrial/commercial carbon loop and mitigating green house gas emissions. However, several bottlenecks presently limit the wide-spread adoption of fuel cells, chiefly, the high cost of the catalyst material – typically Pt. Herein, we demonstrate the effective modification of commercially available 20% Pt/C with an organic ionic plastic crystal (OIPC), tetrabutylphosphonium bis(trifluoromethylsulfonyl)imide ($P_{4444}NTf_2$), layer. With the addition of 2% $P_{4444}NTf_2$@Pt/C a 2.5× increase in the oxidation current of FA was observed. Most contemporary catalysts rely on much greater Pt loadings to achieve similar electrocatalytic

enhancement; therefore, this strategy, while still relying on Pt as a catalyst material, means less Pt needs to be used, reducing the overall cost.

2.3 Introduction

Due to rising environmental concerns, carbon neutral or carbon negative strategies are being sought and a wide range of clean energy-producing technologies are being developed to meet the demand [1-4]. Fuel cells are considered one of the cleanest power sources due to low emissions, high theoretical efficiency, and simplicity; however, they cannot yet compete economically with conventional energy technologies, except in some niche areas [5]. Fuel cells based on FA oxidation are promising owing to their high theoretical energy density and relatively simple two-electron oxidation reaction on Pt [1-4, 6, 7] or Pd [8] catalysts, which occurs through either of two mechanisms: direct (dehydrogenation) or indirect (dehydration) [2, 9-13]. The direct pathway is generally faster and proceeds *via* the formation of an adsorbed active intermediate (equation 1). The indirect pathway occurs by first forming adsorbed CO (CO_{ads}) *via* a chemical dehydration step, which is subsequently oxidized to CO_2 (equation 2).

$$HCOOH_{aq} \rightarrow HCOOH_{ads} \rightarrow 2H^{+} + 2e^{-} + CO_2 \qquad [1]$$

$$HCOOH_{aq} \rightarrow HCOOH_{ads} \rightarrow CO_{ads} + H_2O \rightarrow 2H^{+} + 2e^{-} + CO_2 \qquad [2]$$

The most significant barriers to the widespread FA fuel cell commercialization include, limited durability, inadequate power density, high fuel crossover rate, and the high cost of noble metal catalyst materials [2-4, 14]. Indeed, the use of Pt-based catalysts has dominated the field and has been studied extensively [2, 14]. However, CO_{ads} [6, 10, 12-15] and oxygenated [7, 16] species (*e.g.*, OH_{ads}) have been identified as major causes of chemically blocking Pt active sites. Two general strategies have arisen to improve fuel cell performance while reducing costs: (1) the development of non-precious metal catalysts and (2) surface modification [7, 16-18] or alloying of Pt nanoparticles (NPs) with other metals [12, 15, 19] to reduce the overall amount of Pt required while increasing efficiency [2, 14].

Recently, modification of Pt NPs using IL for electrocatalysis has attracted a great deal of attention [7, 18, 20]. IL are large organic salts with melting points below 100 °C [20-22] and are characterized by their excellent electrochemical and thermal stability. IL have been used as a reaction medium/catalyst [23-25] and supporting electrolytes [26-28], as well as dispersion mediums for NPs and colloids [29-31]. By coating the catalyst with an IL material, the so-called "solid catalyst with ionic liquid layer" (SCILL) is generated [20, 32-34] and several research groups have exemplified this approach. Snyder *et al*. [18] demonstrated the success of impregnating a Ni-Pt alloy NP catalyst with a protic IL with high O_2 solubility to catalyze the O_2 reduction reaction (ORR). Similarly, Tan *et al*. [16] modified the catalytic behavior of Pt NPs grown on graphene nanosheets by adding a layer of IL generated from protonated 7-methyl-1,5,7-triazabicyclo[4.4.0]dec-5-ene (MTBD) and the bis(trifluoromethylsulfonyl)imide anion (NTf_2), which enhanced ORR and inhibited access of methanol to the electrode surface, making it an excellent cathode material for direct methanol fuel cells (DMFC). Finally, Zhang *et al*. [7] modified the surface of commercially available Pt NPs on a carbon support (Pt/C) using the IL, 1-butyl-3-methylimidazolium bis(trifluoromethylsulfonlyl)imide ($C_4C_1ImNTf_2$), and observed a 3 fold improvement in mass-specific-activity (MSA) versus the unmodified catalyst towards ORR that was stable over 30,000 cycles. While the SCILL strategy is relatively new, these works demonstrate its effectiveness and with the vast array of IL possible, they only scratch the surface.

Meanwhile, the field of OIPC, a sub-class of IL, has been relatively unexplored. OIPC are characterized by melting points (T_m) above room temperature; multiple solid-solid phase transitions (T_{ss}) below the melt, presenting a more disordered solid lattice with a concomitant increase in temperature; good ionic conductivity; and are relatively amendable to deformation (*i.e.*, good plasticity) [35, 36]. They have been proposed as solid-state electrolytes for lithium ion batteries [37] and polymer electrolyte membrane fuel cells [38]. While there are still questions concerning the ion conduction mechanism within OIPC [28, 35-42], operating in the solid phase affords some advantages including greater stability and mitigating loss of material to the solution phase, which is critical in a flow cell configuration.

Herein, an alkylphosphonium-based OIPC, tetrabutylphosphonium bis(trifluoromethylsulfonyl)imide ($P_{4444}NTf_2$), was employed to modify the surface of commercial Pt/C catalyst. Alkylphosphonium salts have excellent hydrophobicity [43] as well as thermal and electrochemical stability [21, 22, 28]. The NTf_2 anion is similarly hydrophobic [44] and has been used in multiple SCILL investigations [7, 16]. $P_{4444}NTf_2$ was found to have a $T_m = 85$ °C with one solid-solid phase transition below the melt meaning it should coat the Pt/C surface with a solid layer. The addition of 2 mass % of the OIPC elicited a 2.5× improvement in FA oxidation current versus the unmodified Pt/C. Since $P_{4444}NTf_2$ forms a thin, solid phase on the surface of the commercial catalyst, we introduce the concept of “solid catalyst with organic ionic plastic crystal layer” (SC-OIPC).

2.4 Experimental Section

2.4.1 Materials and synthesis

All chemicals were used as received without further purification, unless indicated otherwise. The Pt/C catalyst (20% on XC-72R carbon black) was obtained from E-Tek. Tributylphosphonium (≥93.5%), 1-bromobutane (≥98%), lithium bis(trifluoromethylsulfonyl)imide ($LiNTf_2$, 99.95%), and FA (FA, 98-100%) were purchased from Sigma-Aldrich. 5% Nafion™ solution was bought from DuPont, while dichloromethane (≥99.5%), acetone (≥99.5%), and 2-propanol (≥99.5%) were obtained from ACS. Sulfuric acid (95-98%) was sourced from Caledon Laboratories Ltd and chloroform-D (99.8%) was purchased from Cambridge Isotope Laboratories, Inc. All aqueous solutions were prepared using ultra-pure MilliQ water (>18.2 MΩ cm).

Tetrabutylphosphonium bis(trifluoromethylsulfonyl)imide [$P_{4444}NTf_2$], was synthesized in a procedure detailed elsewhere [26, 28, 45]. Briefly, tributylphosphonium bromide ($P_{4444}Br$) was first prepared by addition of 1-bromobutane and tributylphosphine to a pressure tube (ACE glass) under N_2 atmosphere and maintained at ~65 °C overnight; an excess 1-bromobutane was added to ensure complete reaction and then removed under reduced atmosphere. A clear, viscous liquid was obtained and confirmed to be $P_{4444}Br$ *via* NMR [45]. Subsequently, equimolar amounts (1:1) of $P_{4444}Br$ and lithium bis(trifluoromethylsulfonyl)imide ($LiNTf_2$) were combined in a ~50/50 (v/v) mixture of water/dichloromethane and allowed to stir overnight at room temperature. The organic phase was collected and washed 3×~100 mL of water. The organic phase was removed under vacuum, and the resultant white solid dried under a high vacuum at ~95 °C for 12 h. To ensure complete removal of impurities and water, it was further recrystallized from ethanol and dried under a high vacuum for 24 h. The final product was a white crystalline solid that was structurally confirmed through ^{1}H and ^{13}C NMR.

2.5 Instrumentation:

Scanning Electron Microscopy (SEM) equipped with Energy Dispersive X-ray (EDX) spectroscopy was used to provide elemental identification using a FEI Quanta 400 equipped with a Bruker 4th generation XFlash SSD X-ray detector. Transmission electron microscopy (TEM) images were acquired using a Tecnai Spirit transmission electron microscope. TEM grids were prepared by drop-casting a catalyst powder dispersion in water on 200 mesh Cu ultrathin/lacey carbon grids (Electron Microscopy Sciences) and allowed to dry in air.

TGA was performed using a TA instrument Q500 thermogravimetric analyzer using a platinum pan and N_2 as balance gas with a flow rate of 50 mL min^{-1}. Initially, all samples were heated to 100 °C for 3 h and cooled to room temperature in a desiccator to eliminate mass loss due to water. During analysis, samples were heated from room temperature to 800 °C at a rate of 10 °C min^{-1} in air.

^{1}H spectra were measured using a Bruker Avance 500 MHz spectrometer in $CDCl_3$. ^{1}H NMR (500 MHz, $CDCl_3$) δ 2.15 – 2.06 (m, 8H), 1.48 (m, 16H), 0.99 – 0.91 (t, 12H). See the Appendix A for more detail.

The Mettler-Toledo DSC, model DSC1 was used to investigate thermal behaviour of the OIPC. Two identical 40 μL aluminum pans (reference and sample) were used and sealed with a pinhole at the top. Samples were initially heated to 150 °C in isothermal temperature mode for 3 min (drying step) to remove any volatile contaminants and any absorbed water from the atmosphere, followed by cooling to –80 °C; subsequently a dynamic temperature scan was conducted from –80 to 150 °C and back at a rate of 2 °C min^{-1}. A constant N_2 gas flow of 50 mL min^{-1} was applied throughout DSC measurements.

An SP-50 potentiostat controlled by EC-Lab software (BioLogic) was employed to record cyclic voltammetric (CV) measurements in a three-electrode cell with a Pt wire, glassy carbon electrode (GCE), and saturated calomel electrode (SCE) as counter, working, and reference electrodes, respectively. All electrochemical measurements were carried out in a N_2 saturated 1.0 M H_2SO_4 solution. The working electrode was manually polished using a 0.3 µm alumina suspension (Buehler Inc.) on a polishing pad followed by ultrasonication in an acetone/water bath for 30 min and dried at room temperature. Electrode surfaces were visually inspected after polishing.

The catalyst coated electrodes were prepared by adding 2.0 mg of catalyst to a mixture of 60% of H_2O, 15% of 2-propanol, and 25% Nafion solution and sonicated for 30 min. Subsequently, 3.0 µL of the resulting ink was drop-cast onto a clean, polished 0.071 cm^2 inlaid disk GCE and allowed to dry in air at room temperature.

2.6 Preparation of OIPC-modified Pt/C catalysts:

The commercial 20% Pt/C catalyst was dispersed in 15 mL of 2-propanol for 30 min by sonication. In a second vial, a predefined amount of $P_{4444}NTf_2$ was dissolved in 5 mL of 2-propanol and kept at room temperature under intense stirring for 30 min. The solutions were then combined. To ensure complete intrusion of the OIPC into the catalyst's pores, the suspension was kept with intense magnetic stirring for 3 h. The resulting suspension was left at room temperature until the volume was reduced to half. After a 30 min ultrasonic treatment, the excess 2-propanol was removed from the suspension using a rotary evaporator (IKA) at 60 °C. Finally, the OIPC@Pt/C catalyst was dried in an oven at 45 °C for 48 h, followed by drying under high vacuum conditions at room temperature to ensure complete removal of the solvent. The OIPC loading is defined as,

$$\text{mass\% OIPC} = \frac{m_{\text{OIPC}}}{m_{\text{catalyst}} + m_{\text{OIPC}}} \times 100\% \tag{3}$$

Where m_{OIPC} is the initial mass of OIPC and m_{catalyst} is the initial mass of unmodified Pt/C catalyst. This mixture was then employed to generate ink (see above) for drop-casting onto GCEs.

2.7 Results and discussion

Figure 2.1A shows cyclic voltammograms (CV) recorded using the unmodified commercial Pt/C catalyst (blue, dashed trace) and after modification with 2 mass % $P_{4444}NTf_2$ (2% OIPC@Pt/C, solid, red trace) deposited on a glassy carbon electrode (GCE) while immersed in 1.0 M H_2SO_4 aqueous electrolyte solution at a scan rate of 100 mV s^{-1}. Both CVs exhibit characteristic waves for H^+ adsorption/desorption on the Pt surface in the potential range of –0.25 to 0.1 V. The current signal in the region >0.6 V is associated with the adsorption of reactive oxygen species (*e.g.*, OH_{abs}) and is decreased upon modification of the catalyst material with OIPC. Oxygenated species inhibit Pt electroactivity; whereby, the suppression of oxygenated species adsorption agrees well with recent reports of IL modified Pt/C catalysts employed for O_2 reduction [7, 16]. An anodic and cathodic peak was observed at ~0.35 V on the forward and reverse scan, respectively, for both the Pt/C and OIPC@Pt/C catalysts, which is indicative of the oxidation/reduction of quinone moieties on the activated carbon surface [46, 47]. However, for the OIPC@Pt/C modified catalyst, this peak intensity was comparatively smaller relative to Pt/C. The smaller peak intensity may be owing to the low diffusivity, activity, or solubility of H_2O/H_3O^+ in the OIPC phase [48] inhibiting quinone formation and redox behaviour. Hydroquinone formation is facilitated by solvation which will be inhibited by the solid OIPC layer.

Decreasing the potential scan rate in the absence of FA to 10 mV s^{-1}, to match the rate used for FA oxidation (see below), causes the current for the surface processes discussed above to decrease relative to the current in the hydrogen evolution and reoxidation region from ca. –0.20 to –0.25 V (see Figure A2 in the Appendix A). Modification of the Pt/C with OIPC caused the maximum current (at –0.25 V) for the H_2 evolution reaction (HER) to increase from –30.9 to –80.0 A mg^{-1} Pt, while the intensity of the H_2 reoxidation peak increased from 11.5 to 55.4 A mg^{-1} Pt. IL are supramolecular fluids that create a hydrophobic microenvironment surrounding the Pt NPs, while simultaneously the NTf_2^- anionic component is a weak Brønsted base [49]. Ion conductivity in OIPC is still an open question [36, 50]; however, it is possible that ion mobility is enhanced along defect sites in the crystal lattice and along grain boundaries of the heterogeneous, polycrystalline OIPC [40, 42]. It is also possible that H^+ mobility occurs through exchange between NTf_2^- moieties similar to triflimide intermolecular stabilization of the proton [49, 51]; however, this is likely minor.

Residual H_2O may be a contributor; however, it is most likely minor owing to the hydrophobicity of the OIPC and since H_2O would inhibit proton adsorption at the Pt NP surface through the formation of hydronium ions ($H(H_2O)_n^+$) [52-54]. This agrees well with recent reports of electrocatalyzed O_2 reduction and H_2 evolution at IL modified NP surfaces [17, 20, 32, 52, 55]. Hydrophobicity of the OIPC was confirmed using static water-contact-angle (WCA) measurements of a thin-film of 2% OIPC@Pt/C drop-cast onto a glass slide (see Figure A1 of the Appendix A). A WCA of 132° was observed indicating good hydrophobicity [7], while a layer of commercial Pt/C was entirely wetting (data not shown).

Figure 2.1B illustrates the CVs recorded in a solution of 0.1 M HCOOH for the 2% OIPC@Pt/C (red, solid trace) and unmodified Pt/C (blue, dashed curve). In the forward scan, two anodic peaks were observed with the first at 0.31 and 0.34 V (peak 1f) with peak intensities of 15.5 and 28.2 A mg^{-1} Pt for the Pt/C and 2% OIPC@Pt/C modified electrodes, respectively. The second peak was recorded at 0.62 and 0.63 V (peak 2f) where 33.1 and 61.7 A mg^{-1} Pt were the current intensities for the Pt/C and 2% OIPC@Pt/C, respectively. When the potential was scanned back towards negative potentials, only one anodic peak was observed for each case at 0.31 and 0.37 V (peak 1b) with currents of 27.4 and 70.7 A mg^{-1} Pt, for Pt/C and 2% OIPC@Pt/C, respectively. The low anodic currents (peak 1f) during the forward scan is owing to CO adsorption onto Pt active sites inhibiting the direct FA oxidation pathway; however, at high overpotentials CO is readily oxidized (peak 2) at ~0.6 V such that, after scanning to these potentials, the Pt surface is relatively pristine and the direct pathway can be accessed during the reverse scan, resulting in higher peak currents (peak 1b) when the potential is scanned back [11, 15, 56, 57]. For both FA and CO oxidation peaks, during the forward scan a ~1.8× increase in current intensity was recorded moving from the bare Pt/C to OIPC@Pt/C catalyst, while during the reverse scan CO oxidation was absent and a 2.5× increase in FA oxidation was observed for the OIPC@Pt/C. The large enhancement of 1b (direct pathway) is particularly important for fuel cell applications where the anode must operate at low overpotentials to provide maximum efficiency. Addition of 5 or 10% $P_{4444}NTf_2$ to the commercial Pt/C catalyst (see Figure A2 in the Appendix A) resulted in a decrease in the effective electrocatalytic activity towards FA oxidation, relative to 2% $P_{4444}NTf_2$, such that peak

1b on the reverse scan reached 41.5 and 35.0 A mg^{-1} Pt at ~0.40 V, respectively. Additional OIPC likely creates increased complexity in the polycrystalline structure disrupting ion/molecular conduction pathways that limit FA access to the Pt NP surface [42]. However, these results still represent a modest increase versus the unmodified catalyst, albeit at higher overpotentials.

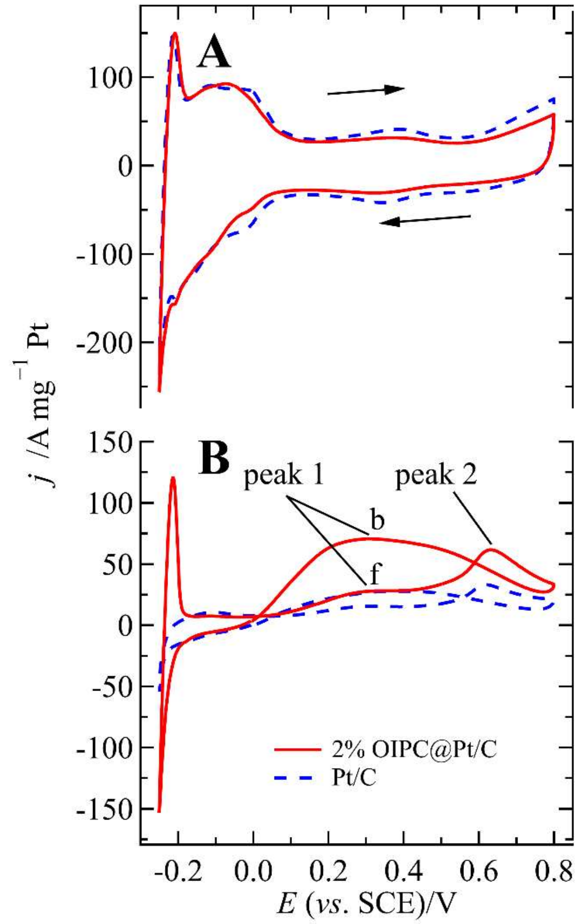

Figure 2.1: Cyclic voltammograms (CV) plotted in terms of current density per mg of Pt catalyst employed for commercial Pt/C (blue, dashed curve) and 2 wt.% OIPC@Pt/C (solid, red trace) modified GCEs, recorded in N_2 saturated 1.0 M H_2SO_4 aqueous electrolyte solution before [A] and after [B] addition of 0.1 M HCOOH. CVs in A and B were performed at scan rates of 100 and

10 mV s^{-1}, respectively. Arrows indicate scan direction, while f = forward and b = backward scan direction in B where CVs crossover.

The 2.5× increase in FA oxidation current at 0.37 V for the 2% OIPC@Pt/C versus the Pt/C catalyst is significant and represents a fundamental shift in reactivity. The extensive literature on FA oxidation at Pt NP has demonstrated that activities can be influenced by surface coatings in a number of different ways [58-60]. These include: third body effects in which adsorbed species can inhibit formation of the poisoning CO_{ads} intermediate by limiting the number of contiguous Pt sites; changes in morphology; electronic (ligand) effects which can decrease the strength of CO adsorption and/or promote Pt-OH formation; influences on the orientation of the FA molecule such as changes in hydration [61, 62]; more specific interactions with the FA molecule [60, 63]. The involvement of significant third body effects [64] can be eliminated here because the CVs in Fig. 2.1A show an insignificant change in the area under the H desorption peaks between ca. –0.2 and +0.1 V, indicating that there was very little blocking of Pt sites by the OIPC. It is likely that the OIPC behaves similarly to a polymer modified surface [60, 65] such that hydrophobic domains exist within polycrystalline grain boundaries that favour entry and diffusion of FA. In the polymer case, these domains can exclude H_2O and influence the orientation in which FA approaches the Pt NPs interface; *i.e.*, C-H down which favours the direct pathway [65]. However further characterization of the nature of the OIPC/Pt interface is necessary to elucidate the relative importance of the other mechanisms.

To investigate whether the OIPC modified the morphology of the Pt NPs, TEM images were taken (Figure 2.2) in which black, spherical Pt particles are seen to be spread homogeneously on the carbon support in the case of both the unmodified and OIPC modified Pt/C catalyst. Roughly

150 random particles were measured using ImageJ software for both cases and compiled into the histograms shown inset in Figure 2.2. Both histograms were fit using a Gaussian distribution (red trace) and an average NP diameter of 3.18 and 3.25 nm were determined using the peak from each curve fitting. These data suggest that there was no significant size or morphological change relative to the unmodified Pt NPs, nor any observable change in their distribution across the surface of the carbon support.

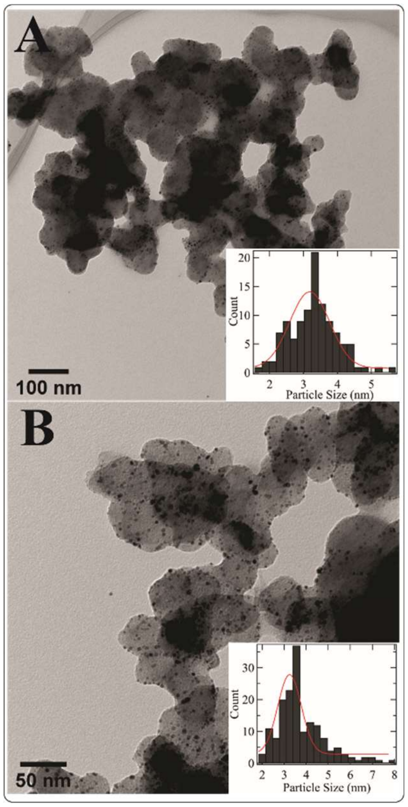

Figure 2.2: TEM micrographs of a) unmodified Pt/C and b) the 2% OIPC@Pt/C catalyst. Inset are histograms of their respective particle sizing.

Next, the catalyst materials were analyzed using TGA to explore interactions between the OIPC and Pt NP. In Figure 2.3A and inset 3(a), as the temperature increased, a mass loss of ~4.6% was observed for 5% OIPC@Pt/C (red trace) in the range of 20-160 °C with an abrupt drop at ~150 °C, while 2% OIPC@Pt/C (blue curve) and Pt/C (green curve) undergo a gradual mass loss in the same region of ~2.5%. For the OIPC modified catalysts, the mass loss in these regions agrees roughly with the amount of OIPC added, while for Pt/C this can likely be attributed to thermal loss of labile oxygen from quinone and other (e.g. -OH, -CO_2H) moieties on the activated carbon support [16, 46]. Proceeding to higher temperatures, gradual mass loss was observed from 160 to 370 °C; however, above 400 °C, a drop in mass was observed for Pt/C, 2% OIPC@Pt/C, and 5% OIPC@Pt/C with onset temperatures of roughly 375, 395, and 465 °C, with final residual masses of 19.0, 18.5, and 19.0%, respectively. The residual masses agree well with Pt composition of the commercial catalyst (20%, see Table A1 in the Appendix A). The presence of OIPC shifts the onset of thermal decomposition to higher temperatures indicating that the OIPC thermally stabilizes the carbon support. Figure 2.3B shows a comparison of thermograms obtained using activated carbon (black curve) and $P_{4444}NTf_2$ itself (red trace), as well as 5 and 20% OIPC (green and blue traces, respectively) on activated carbon. $P_{4444}NTf_2$ containing samples undergo thermal decomposition beginning at roughly 280-300 °C, while the 5 and 20% OIPC/C samples showed a mass loss of 3.6 and 16.7%, respectively, in that region, which roughly agrees with the mass of OIPC added. Interestingly, activated carbon does not show significant loss up to 580 °C. Phosphonium IL/OIPC are known to be highly thermally stable [21, 22]; however, in the case of Pt/C modified catalyst, the presence of Pt NPs appears to catalyze thermal decomposition of the OIPC (and the carbon support). This indicates that there is significant interaction between the OIPC and Pt NPs, which may contribute to its effect on FA oxidation.

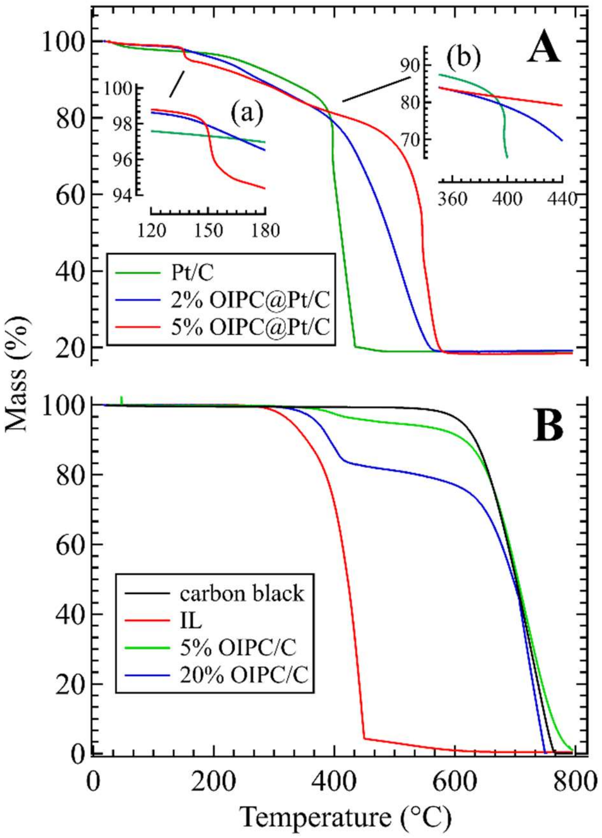

Figure 2.3: Thermograms recorded for [**A**] the commercial Pt/C catalyst unmodified and modified as indicated inset, as well as [**B**] for carbon black, the IL $P_{4444}NTf_2$ itself, and the IL on carbon black as described inset. All were performed in air at a heating rate of 10 °C min^{-1}.

The DSC thermograph of $P_{4444}NTf_2$ (see inset in Figure 2.4 and Figure A4 of the Appendix A) exhibits two endothermic peaks corresponding to T_m at 85°C and a solid-solid phase transition (T_{ss}) at 58°C. No glass-transition temperature was observed down to –80 °C. This indicates that $P_{4444}NTf_2$ likely forms a solid layer on the surface of the Pt/C catalyst. To investigate this further, SEM imaging was employed. SEM micrographs of 2% OIPC@Pt/C and Pt/C on carbon conductive tabs have been presented in Figure 2.4A and B, respectively. The unmodified Pt/C possesses a distinct surface roughness that is absent in the IL modified catalyst (Figure 2.4A and B). The smoothed surface in the latter is likely due to the formation of the OIPC layer.

Zhang *et al*. [7] recently showed that the addition of 18 wt.% of their IL, $C_4C_1ImNTf_2$, enhanced the hydrophobicity of commercial Pt/C catalyst as evidenced through static WCA measurements, changing the WCA from a completely wetting surface for unmodified Pt/C, to a 110° WCA hydrophobic one with Pt/C-$C_4C_1ImNTf_2$. They also showed that their IL@Pt/C system decreased the amount of adsorbed reactive oxygen species (*e.g.*, OH_{abs}) [7], protecting the Pt NPs and enhancing the kinetics of ORR electrocatalysis.

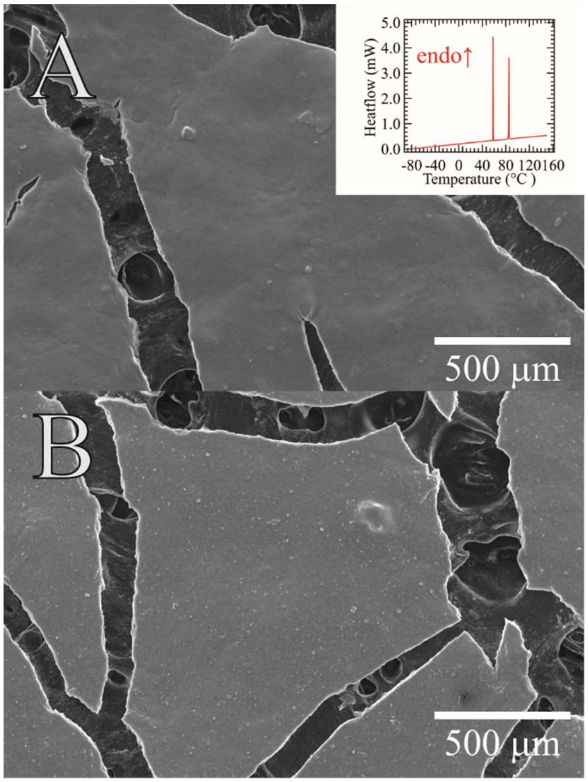

Figure 2.4: SEM micrographs of [**A**] 2% OIPC@Pt/C and [**B**] unmodified Pt/C catalyst layered on a carbon conductive tabs. Inset is a DSC thermogram of $P_{4444}NTf_2$ recorded at a heat rate of 2 °C min^{-1}.

According to the Nernst equation for the HER in acidic media, the catalytic performance of Pt based catalyst can be improved by increasing the surrounding proton activity [52, 66]. In a SCILL system, the activity and selectivity depend upon the amount/thickness of the IL layer and type of IL used, which influences ionic mobility [7, 17, 18, 34, 52]. Typically, protic IL/OIPC are employed owing to their enhanced proton mobility [36, 47, 52, 55, 67-73], *e.g.*, through proton exchange processes like the Grotthus mechanism (proton hopping); however, $P_{4444}NTf_2$ is not a protic salt. Romanenko *et al*. [42] investigated ion transport within a similar OIPC, methyltriethylphosphonium bis(fluorosulfonyl)imide ($P_{1222}FSI$), using 3D solid-state magnetic resonance imaging (MRI) revealing that the size and orientation of the polycrystalline phase influences ion transport which is in turn affected by the rate of cooling – the co-called 'thermal history'. However, their work focuses on the rapid or slow cooling of the bulk OIPC, while herein, the OIPC was essentially recrystallized from isopropanol onto the Pt/C surface on a relatively small scale. Similarly, Zhu *et al*. [40] investigated the ion transport within two protic imidazolium OIPC paired with the triflate anion, in which one imidazolium cation possessed two labile protons and the second had one of these replaced with a methyl group. In the former, the group evidenced that proton conduction occurred within the solid-state *via* proton hopping; however, for the methylated imidazolium it was likely through 'vehicular motion' along grain boundaries involving movement of both cationic and anionic components of the OIPC [40]. The observed current enhancement can be explained using the polycrystalline OIPC model of grain boundary ion/molecular transport proposed by Forsyth's group [40, 42]. Additionally, the hydrophobic, polymer modified catalyst interface described by Wang and Liu [65] in which FA orientation towards the Pt NP surface favours the direct pathway, may be mirrored here in the OIPC case as well. Water exclusion from the grain boundary environment may also explain the enhanced H_2 evolution reaction (HER) current observed for the OIPC modified catalyst.

Based on these results, OIPC@Pt/C limits adsorption of CO and oxygenated species and seems to stabilize Pt NPs. While repeated cycling of the cell is necessary to demonstrate its long-term stability, this is beyond the scope of the present work. However, because the OIPC is a solid layer, leaching of material is expected to be lower than for IL.

2.8 Conclusion

Herein, we have demonstrated the formation of a solid OIPC layer composed of $P_{4444}NTf_2$ that can be installed on the surface of commercial Pt/C catalyst for improved electrocatalyst performance towards FA oxidation. SEM images show the distinct formation of a solid layer on the surface of OIPC@Pt/C catalyst, while DSC measurements indicate that $P_{4444}NTf_2$ is solid up to 85 °C with one solid-solid phase transition below the melt. These results indicate $P_{4444}NTf_2$ possesses two plastic, solid phases from 58-85 °C and <58 °C with no observable glass transition within the available range. Interestingly, while $P_{4444}NTf_2$ is not a protic ionic crystal, the OIPC@Pt/C demonstrates improved HER in the –0.20 to –0.25 V region versus the unmodified commercial catalyst. This may indicate good solid-state ionic conductivity; however, while questions remain about the mechanism of ion or HCOOH mobility, it is likely along grain boundaries of the polycrystalline OIPC that in turn influence the microenvironment in the vicinity of the Pt/OIPC interface. This may also improve the orientation with which FA approaches the Pt surface favouring the direct pathway, similar to polymeric modifications [60, 65]. Nevertheless, the 2.5× current enhancement by OIPC modification towards FA oxidation is highly significant and warrants further investigation, particularly since $P_{4444}NTf_2$ is aprotic.

By modifying a commercial Pt NP catalyst with a solid layer, leaching or erosion of NPs can hopefully be mitigated while simultaneously the adsorption of interfering chemical species (*e.g.*, CO and OH) can be blocked.

2.9 Acknowledgements

TJS is grateful to the Natural Sciences and Engineering Research Council (NSERC) of Canada for funding *via* a Discovery Grant (#006074-2019) and Supplementary Accelerator Grant, as well as Memorial University for funding.

2.10 References

[1] S. Kar, A. Goeppert, G.K.S. Prakash, Integrated CO_2 Capture and Conversion to Formate and Methanol: Connecting Two Threads, Acc. Chem. Res., 52 (2019) 2892-2903.

[2] Z. Ma, U. Legrand, E. Pahija, J.R. Tavares, D.C. Boffito, From CO_2 to Formic Acid Fuel Cells, Industrial & Engineering Chemistry Research, 60 (2021) 803-815.

[3] X. Ren, Y. Wang, A. Liu, Z. Zhang, Q. Lv, B. Liu, Current Progress and Performance Improvement Of Pt/C Catalysts for Fuel Cells, J. Mater. Chem. A, 8 (2020) 24284-24306.

[4] X. Ren, Q. Lv, L. Liu, B. Liu, Y. Wang, A. Liu, G. Wu, Current Progress of Pt and Pt-Based Electrocatalysts used for Fuel Cells, Sustainable Energy & Fuels, 4 (2020) 15-30.

[5] T.d.S. Almeida, A.R. De Andrade, Chapter 15 - New Trends in Direct Ethanol Fuel Cells, in: S.L. Suib (Ed.) New and Future Developments in Catalysis, Elsevier, Amsterdam, 2013, pp. 429-452.

[6] K.A. Schwarz, R. Sundararaman, T.P. Moffat, T.C. Allison, Formic Acid Oxidation on Platinum: A Simple Mechanistic Study, Phys. Chem. Chem. Phys., 17 (2015) 20805-20813.

[7] G.-R. Zhang, M. Munoz, B.J.M. Etzold, Accelerating Oxygen-Reduction Catalysts through Preventing Poisoning with Non-Reactive Species by Using Hydrophobic Ionic Liquids, Angew. Chem. Int. Ed., 55 (2016) 2257-2261.

[8] T. Shen, J. Zhang, K. Chen, S. Deng, D. Wang, Recent Progress of Palladium-Based Electrocatalysts for the Formic Acid Oxidation Reaction, Energy & Fuels, 34 (2020) 9137-9153.

[9] X. Zhao, Y. Hu, L. Liang, C. Liu, J. Liao, W. Xing, Ionic Liquid-Mediated Synthesis of 'Clean' Palladium Nanoparticles for Formic Acid Electrooxidation, Int. J. Hydrogen Energy, 37 (2012) 51-58.

[10] Q. Zhang, A. Sayadi, P.G. Pickup, Separation of Kinetic and Mass Transport Effects In The Electrolysis Of Formic Acid in a Flow-Through Cell, Electrochim. Acta, 294 (2019) 110-116.

[11] A. Sayadi, P.G. Pickup, Electrochemical Oxidation of Formic Acid at Carbon Supported Pt Coated Rotating Disk Electrodes, Russ. J. Electrochem., 53 (2017) 1054-1060.

[12] E.N. El Sawy, P.G. Pickup, Formic Acid Oxidation at Ru@Pt Core-Shell Nanoparticles, Electrocatal, 7 (2016) 477-485.

[13] R.B. Moghaddam, P.G. Pickup, Mechanistic Studies of Formic Acid Oxidation at Polycarbazole Supported Pt Nanoparticles, Electrochim. Acta, 111 (2013) 823-829.

[14] Z. Fang, W. Chen, Recent Advances in Formic Acid Electro-Oxidation: from the Fundamental Mechanism to Electrocatalysts, Nanoscale Advances, 3 (2021) 94-105.

[15] E.N. El Sawy, P.G. Pickup, Carbon monoxide and Formic Acid Oxidation at Rh@Pt Nanoparticles, Electrochim. Acta, 302 (2019) 234-240.

[16] Y. Tan, C. Xu, G. Chen, N. Zheng, Q. Xie, A Graphene–Platinum Nanoparticles–Ionic Liquid Composite Catalyst for Methanol-Tolerant Oxygen Reduction Reaction, Energy Environ. Sci., 5 (2012) 6923-6927.

[17] G.-R. Zhang, B.J.M. Etzold, Ionic Liquids in Electrocatalysis, J. Energy Chem., 25 (2016) 199-207.

[18] J. Snyder, T. Fujita, M.W. Chen, J. Erlebacher, Oxygen Reduction in Nanoporous Metal–Ionic Liquid Composite Electrocatalysts, Nature Mater., 9 (2010) 904-907.

[19] R.M. Altarawneh, P.G. Pickup, Pt and PtRu Catalyst Bilayers Increase Efficiencies for Ethanol Oxidation in Proton Exchange Membrane Electrolysis and Fuel Cells, J. Power Sources, 366 (2017) 27-32.

[20] O. Bartlewicz, I. Dąbek, A. Szymańska, H. Maciejewski, Heterogeneous Catalysis with the Participation of Ionic Liquids, Catalysts, 10 (2020) 1227.

[21] G. Adamova, R.L. Gardas, M. Nieuwenhuyzen, A.V. Puga, L.P.N. Rebelo, A.J. Robertson, K.R. Seddon, Alkyltributylphosphonium Chloride Ionic Liquids: Synthesis, Physicochemical Properties and Crystal Structure, Dalton Trans., 41 (2012) 8316-8332.

[22] G. Adamova, R.L. Gardas, L.P.N. Rebelo, A.J. Robertson, K.R. Seddon, Alkyltrioctylphosphonium Chloride Ionic Liquids: Synthesis and Physicochemical Properties, Dalton Trans., 40 (2011) 12750-12764.

[23] J.-M. Xu, B.-K. Liu, W.-B. Wu, C. Qian, Q. Wu, X.-F. Lin, Basic Ionic Liquid as Catalysis and Reaction Medium: A Novel and Green Protocol for the Markovnikov Addition of N-Heterocycles to Vinyl Esters, Using a Task-Specific Ionic Liquid, [bmIm]OH, J. Org. Chem., 71 (2006) 3991-3993.

[24] Y. Zhang, B. Zhen, H. Li, Y. Feng, Basic Ionic Liquid as Catalyst and Surfactant: Green Synthesis of Quinazolinone in Aqueous Media, RSC Adv., 8 (2018) 36769-36774.

[25] A. Banerjee, R.W.J. Scott, Optimization of Transition Metal Nanoparticle-Phosphonium Ionic Liquid Composite Catalytic Systems for Deep Hydrogenation and Hydrodeoxygenation Reactions, Green Chem., 17 (2015) 1597-1604.

[26] R. Moshrefi, A. Suryawanshi, T.J. Stockmann, Electrochemically Controlled Au Nanoparticle Nucleation At A Micro Liquid/Liquid Interface Using Ferrocene as Reducing Agent, Electrochem. Commun., 122 (2021) 106894.

[27] Q. Jiang, H.E. Reader, T.J. Stockmann, Electrochemical Characterization of Fe(II) Complexation Reactions at an Electrified Micro Liquid-Liquid Interface, ChemElectroChem, 8 (2021) 1580-1587.

[28] T.J. Stockmann, P.D. Boyle, Z. Ding, Preparation and Crystal Structure of Tetraoctylphosphonium Tetrakis(Pentafluorophenyl)Borate Ionic Liquid for Electrochemistry at its Interface with Water, Catal. Today, 295 (2017) 89-94.

[29] Z. He, P. Alexandridis, Ionic Liquid and Nanoparticle Hybrid Systems: Emerging applications, Adv. Colloid Interface Sci., 244 (2017) 54-70.

[30] Z. He, P. Alexandridis, Nanoparticles in Ionic Liquids: Interactions and Organization, Phys. Chem. Chem. Phys., 17 (2015) 18238-18261.

[31] A. Banerjee, R.W.J. Scott, Au, Ag, and Cu Nanostructures, in: Nanocatalysis in Ionic Liquids, Wiley-VCH, 2016, pp. 97-123.

[32] G.-R. Zhang, T. Wolker, D.J.S. Sandbeck, M. Munoz, K.J.J. Mayrhofer, S. Cherevko, B.J.M. Etzold, Tuning the Electrocatalytic Performance of Ionic Liquid Modified Pt Catalysts for the Oxygen Reduction Reaction via Cationic Chain Engineering, ACS Catalysis, 8 (2018) 8244-8254.

[33] M. George, G.-R. Zhang, N. Schmitt, K. Brunnengräber, D.J.S. Sandbeck, K.J.J. Mayrhofer, S. Cherevko, B.J.M. Etzold, Effect of Ionic Liquid Modification on the ORR Performance and Degradation Mechanism of Trimetallic PtNiMo/C Catalysts, ACS Catalysis, 9 (2019) 8682-8692.

[34] U. Kernchen, B. Etzold, W. Korth, A. Jess, Solid Catalyst with Ionic Liquid Layer (SCILL) – A New Concept to Improve Selectivity Illustrated by Hydrogenation of Cyclooctadiene, Chemical Engineering & Technology, 30 (2007) 985-994.

[35] J.M. Pringle, Recent Progress in the Development and use of Organic Ionic Plastic Crystal Electrolytes, Phys. Chem. Chem. Phys., 15 (2013) 1339-1351.

[36] H. Zhu, D.R. MacFarlane, J.M. Pringle, M. Forsyth, Organic Ionic Plastic Crystals as Solid-State Electrolytes, Trends Chem., 1 (2019) 126-140.

[37] D.R. MacFarlane, J. Huang, M. Forsyth, Lithium-doped Plastic Crystal Electrolytes Exhibiting Fast Ion Conduction for Secondary Batteries, Nature, 402 (1999) 792-794.

[38] J. Luo, A.H. Jensen, N.R. Brooks, J. Sniekers, M. Knipper, D. Aili, Q. Li, B. Vanroy, M. Wubbenhorst, F. Yan, L. Van Meervelt, Z. Shao, J. Fang, Z.-H. Luo, D.E. De Vos, K.

Binnemans, J. Fransaer, 1,2,4-Triazolium Perfluorobutanesulfonate as an Archetypal Pure Protic Organic Ionic Plastic Crystal Electrolyte for All-Solid-State Fuel Cells, Energy Environ. Sci., 8 (2015) 1276-1291.

[39] C.B. Park, B.J. Sung, Heterogeneous Rotational Dynamics of Imidazolium-Based Organic Ionic Plastic Crystals, J. Phys. Chem. B, 124 (2020) 6894-6904.

[40] H. Zhu, X. Wang, R. Vijayaraghava, Y. Zhou, D.R. MacFarlane, M. Forsyth, Structure and Ion Dynamics in Imidazolium-Based Protic Organic Ionic Plastic Crystals, J. Phys. Chem. Lett., 9 (2018) 3904-3909.

[41] K. Romanenko, J.M. Pringle, L.A. O'Dell, M. Forsyth, New Insights Into The Thermal Behaviour of Organic Ionic Plastic Crystals: Magnetic Resonance Imaging of Polycrystalline Morphology Alterations Induced by Solid-Solid Phase Transitions, Phys. Chem. Chem. Phys., 17 (2015) 18991-19000.

[42] K. Romanenko, L. Jin, L.A. Madsen, J.M. Pringle, L.A. O’Dell, M. Forsyth, Anisotropic MRI Contrast Reveals Enhanced Ionic Transport in Plastic Crystals, J. Am. Chem. Soc., 136 (2014) 15638-15645.

[43] T.J. Stockmann, R. Guterman, P.J. Ragogna, Z. Ding, Trends in Hydrophilicity/Lipophilicity of Phosphonium Ionic Liquids as Determined by Ion-Transfer Electrochemistry, Langmuir, 32 (2016) 12966–12974.

[44] T.J. Stockmann, Z. Ding, Hydrophobicity of Room Temperature Ionic Liquids Assessed By The Galvani Potential Difference Established at Micro Liquid/Liquid Interfaces, J. Electroanal. Chem., 649 (2010) 23-31.

[45] U. Domańska, M. Wlazło, M. Karpińska, M. Zawadzki, New ionic liquid [$P_{4,4,4,4}$][NTf_2] in bio-butanol extraction on investigation of limiting activity coefficients, Fluid Phase Equilib., 475 (2018) 89-94.

[46] V.A. Garten, D.E. Weiss, Quinone-Hydroquinone Character Of Activated Carbon and Carbon Black, Aust. J. Chem., 8 (1955) 68-95.

[47] A.I. Inozemtseva, E.Y. Kataev, A.S. Frolov, M. Amati, L. Gregoratti, K. Beranová, V.P. Dieste, C. Escudero, A. Fedorov, A.V. Tarasov, D.Y. Usachov, D.V. Vyalikh, Y. Shao-Horn, D.M. Itkis, L.V. Yashina, On the Catalytic and Degradative Role of Oxygen-Containing Groups on Carbon Electrode in Non-Aqueous ORR, Carbon, 176 (2021) 632-641.

[48] T. Song, O. Morales-Collazo, J.F. Brennecke, Solubility and Diffusivity of Oxygen in Ionic Liquids, J. Chem. Eng. Data, 64 (2019) 4956-4967.

[49] W. Zhao, J. Sun, Triflimide ($HNTf_2$) in Organic Synthesis, Chem. Rev., 118 (2018) 10349-10392.

[50] I. Popov, K. Biernacka, H. Zhu, F. Nti, L. Porcarelli, X. Wang, A. Khamzin, C. Gainaru, M. Forsyth, A.P. Sokolov, Strongly Correlated Ion Dynamics in Plastic Ionic Crystals and Polymerized Ionic Liquids, J. Phys. Chem. C, 124 (2020) 17889-17896.

[51] A. Haas, C. Klare, P. Betz, J. Bruckmann, C. Krüger, Y.H. Tsay, F. Aubke, Acyclic Sulfur−Nitrogen Compounds. Syntheses and Crystal and Molecular Structures of Bis((trifluoromethyl)sulfonyl)amine ($(CF_3SO_2)_2NH$), Magnesium Hexaaquo Bis((trifluoromethyl)sulfonyl)amide Dihydrate ($[Mg(H_2O)_6][(CF_3SO_2)_2N]_2{\cdot}2H_2O$), and Bis(bis(fluorosulfonyl)amino)sulfur ($(FSO_2)_2NSN(SO_2F)_2$), Inorg. Chem., 35 (1996) 1918-1925.

[52] Q. Wang, Y. Gao, Z. Ma, Y. Zhang, W. Ni, H.A. Younus, C. Zhang, Z. Chen, S. Zhang, Supported Ionic Liquid Phase-Boosted Highly Active and Durable Electrocatalysts Towards Hydrogen Evolution Reaction in Acidic Electrolyte, J. Energy Chem., 54 (2021) 342-351.

[53] J.-X. Feng, S.-Y. Tong, Y.-X. Tong, G.-R. Li, Pt-like Hydrogen Evolution Electrocatalysis on PANI/CoP Hybrid Nanowires by Weakening the Shackles of Hydrogen Ions on the Surfaces of Catalysts, J. Am. Chem. Soc., 140 (2018) 5118-5126.

[54] C.A. Reed, Myths about the Proton. The Nature of H^+ in Condensed Media, Acc. Chem. Res., 46 (2013) 2567-2575.

[55] X. Yan, F. Zhang, H. Zhang, H. Tang, M. Pan, P. Fang, Improving Oxygen Reduction Performance by Using Protic Poly(Ionic Liquid) as Proton Conductors, ACS Appl. Mater. Int., 11 (2019) 6111-6117.

[56] V. Grozovski, J. Solla-Gullón, V. Climent, E. Herrero, J.M. Feliu, Formic Acid Oxidation on Shape-Controlled Pt Nanoparticles Studied by Pulsed Voltammetry, J. Phys. Chem. C, 114 (2010) 13802-13812.

[57] Z.-B. Wang, Y.-Y. Chu, A.-F. Shao, P.-J. Zuo, G.-P. Yin, Electrochemical Impedance Studies of Electrooxidation of Methanol and Formic Acid on Pt/C Catalyst in Acid Medium, J. Power Sources, 190 (2009) 336-340.

[58] A. Boronat-González, E. Herrero, J.M. Feliu, Fundamental Aspects of HCOOH Oxidation at Platinum Single Crystal Surfaces ith Basal Orientations and Modified Bby Irreversibly Adsorbed Adatoms, J. Solid State Electrochem., 18 (2014) 1181-1193.

[59] H. Jeon, B. Jeong, J. Joo, J. Lee, Electrocatalytic Oxidation of Formic Acid: Closing the Gap Between Fundamental Study and Technical Applications, Electrocatal, 6 (2015) 20-32.

[60] R.B. Moghaddam, P.G. Pickup, Influences of Aniline, Carbazole, Indole, and Pyrrole Monomers and Polymers on Formic Acid Oxidation at Pt Electrodes, Electrochim. Acta, 107 (2013) 225-230.

[61] M. Choy M, F. Hahn, J.M. Léger, C. Lamy, J.M. Ortega, In situ Fourier Transformed Infrared Reflectance Spectroscopy Study of the Effect of Poly-Pdmb Film Modified Platinum Electrodes on the Electrooxidation of Formic Acid, Thin Solid Films, 515 (2007) 3611-3618.

[62] H.V. Patten, E. Ventosa, A. Colina, V. Ruiz, J. Lopez-Palacios, A.J. Wain, S.C.S. Lai, J.V. MacPherson, P.R. Unwin, Influence of Ultrathin Poly-(3,4-Ethylenedioxythiophene) (PEDOT) Film Supports on the Electrodeposition and Electrocatalytic Activity of Discrete Platinum Nanoparticles, J. Solid State Electrochem., 15 (2011) 2331-2339.

[63] J.V. Perales-Rondón, A. Ferre-Vilaplana, J.M. Feliu, E. Herrero, Oxidation Mechanism of Formic Acid on the Bismuth Adatom-Modified Pt(111) Surface, J. Am. Chem. Soc., 136 (2014) 13110-13113.

[64] E. Leiva, T. Iwasita, E. Herrero, J.M. Feliu, Effect of Adatoms in the Electrocatalysis of HCOOH Oxidation. A Theoretical Model, Langmuir, 13 (1997) 6287-6293.

[65] H.-F. Wang, Z.-P. Liu, Formic Acid Oxidation at Pt/H_2O Interface from Periodic DFT Calculations Integrated with a Continuum Solvation Model, J. Phys. Chem. C, 113 (2009) 17502-17508.

[66] G.-R. Xu, J. Bai, J.-X. Jiang, J.-M. Lee, Y. Chen, Polyethyleneimine Functionalized Platinum Superstructures: Enhancing Hydrogen Evolution Performance by Morphological and Interfacial Control, Chem. Sci., 8 (2017) 8411-8418.

[67] M. Qiao, G.A. Ferrero, L. Fernández Velasco, W. Vern Hor, Y. Yang, H. Luo, P. Lodewyckx, A.B. Fuertes, M. Sevilla, M.-M. Titirici, Boosting the Oxygen Reduction Electrocatalytic Performance of Nonprecious Metal Nanocarbons via Triple Boundary Engineering Using Protic Ionic Liquids, ACS Appl. Mater. Int., 11 (2019) 11298-11305.

[68] C. Karlsson, C. Strietzel, H. Huang, M. Sjödin, P. Jannasch, Nonstoichiometric Triazolium Protic Ionic Liquids for All-Organic Batteries, ACS Applied Energy Materials, 1 (2018) 6451-6462.

[69] T.L. Greaves, C.J. Drummond, Protic Ionic Liquids: Evolving Structure–Property Relationships and Expanding Applications, Chem. Rev., 115 (2015) 11379-11448.

[70] Y. Shen, D.F. Kennedy, T.L. Greaves, A. Weerawardena, R.J. Mulder, N. Kirby, G. Song, C.J. Drummond, Protic Ionic Liquids With Fluorous Anions: Physicochemical Properties And Self-Assembly Nanostructure, Phys. Chem. Chem. Phys., 14 (2012) 7981-7992.

[71] U.A. Rana, M. Forsyth, D.R. MacFarlane, J.M. Pringle, Toward Protic Ionic Liquid and Organic Ionic Plastic Crystal Electrolytes For Fuel Cells, Electrochim. Acta, 84 (2012) 213-222.

[72] J.B. Rollins, J.C. Conboy, Kinetics and Thermodynamics of Hydrogen Oxidation and Oxygen Reduction in Hydrophobic Room-Temperature Ionic Liquids, J. Electrochem. Soc., 156 (2009) B943.

[73] M. Yoshizawa, W. Xu, C.A. Angell, Ionic Liquids by Proton Transfer: Vapor Pressure, Conductivity, and the Relevance of ΔPKa from Aqueous Solutions, J. Am. Chem. Soc., 125 (2003) 15411-15419.

Chapter 3

Modification of Pt/C with aprotic tetraalkylphosphonium ionic liquid and OIPC for methanol oxidation reaction

3.1 Abstract

The modification of Pt/C catalysts with ionic liquids (IL) to give a so-called ‘solid catalyst with an IL layers’ (SCILL), has been demonstrated as a facile approach to improve catalyst activity. In this work, IL were layered onto a 20% by mass Pt/C nanoparticle commercial catalyst for surface anode modification, for the methanol oxidation reaction (MOR) in fuel cells. Alkyltributylphosphonium bis(trifluoromethylsulfonyl)imide ($P_{444*}NTf_2$) IL, whereby the fourth arm on the phosphonium core was of chain lengths from C-4 to C-8, were investigated. Cyclic voltammetry was employed to assess the electrocatalytic performance of the as-prepared IL@Pt/C catalysts in a conventional 3 electrode cell. Catalyst and IL thermal properties were characterized by thermogravimetric analysis (TGA) and differential scanning calorimeter (DSC); the later revealed that $P_{4444}NTf_2$ is an organic ionic plastic crystal (OIPC) with a melting point of ~85 °C. Catalytic enhancement versus the unmodified Pt/C was only observed for $P_{4444}NTf_2$; indeed, $P_{4446}NTf_2$ and $P_{4448}NTf_2$ modification decreased the overall CH_3OH oxidation currents versus the bare Pt/C catalyst. These works imply IL/OIPC modification can become a powerful technique to improve anodic catalytic performance.

3.2 Introduction

Attempts to find alternative fuels for electricity generation has led to the development of direct alcohol fuel cell (DAFC); mainly, the direct methanol fuel cell (DMFC) due to the high theoretical efficiency (97%) of electrocatalyzed MOR at low temperatures [77,78] as well as the ability to store CH_3OH as a liquid at room temperature [79]. This latter means CH_3OH can be relatively easily incorporated into contemporary gasoline infrastructure which is advantageous compared to hydrogen fuel cells that rely on pressurized tanks to store H_2 gas [80]. Moreover, the volumetric energy density for methanol is 4.82 $kWh.L^{-1}$, higher than that of hydrogen [5], and it has the highest energy production per unit of CO_2 produced versus other alcohols. However, challenges such as fuel cross-over and low catalyst activity restrict commercialization of DMFC [2,6]. Therefore, understanding the mechanistic details of MOR is essential for the further development of DMFC [7]. The electrochemical MOR is described by (equation 1),

$$CH_3OH + H_2O \rightarrow 6H^+ + CO_2 + 6e^- \qquad (1)$$

It produces 6 electrons for complete oxidation to CO_2; however, this is rarely a concerted reaction and often occurs stepwise. In the case where a Pt electrode is used, the first step is methanol adsorption on the surface of a Pt active site,

$$CH_3OH + Pt \rightarrow Pt\text{-}CH_3OH_{ads} \qquad (2)$$

This is followed by platinum-catalyzed electrochemical dehydrogenation,

$$Pt\text{-}CH_3OH_{ads} \rightarrow Pt\text{-}CO_{ads} + 4H^+ + 4e^- \qquad (3)$$

Subsequent CO_{ads} oxidation involves oxygenated species formed by dissociative adsorption of water on an adjacent Pt active site,

$Pt + H_2O \rightarrow Pt\text{-}H_2O_{ads} \rightarrow Pt\text{-}OH_{ads} + H^+ + e^-$ (4)

Lastly, the two adsorbed species react in a Langmuir-Hinshelwood (LH) type of mechanism,

$Pt\text{-}OH_{ads} + Pt\text{-}CO_{ads} + \rightarrow 2Pt + CO_2 + H^+ e^-$ (5)

Mechanisms of this type require high overpotentials (>0.75 V), while the multiple steps decrease the kinetics of the MOR [3,7–10]. The incomplete oxidation of methanol leads to by-products, such as formaldehyde and formic acid, generating fewer electrons than complete oxidation and lowering the overall energy conversion efficiency [11].

Pt-based catalysts are commonly used in fuel cells and have been studied extensively. Modification of Pt catalyst by alloying with oxophilic metals has shown improvement in the electrocatalytic activity for organic fuel oxidation [12,13]. However, aggregation of Pt nanoparticles, poisoning of the catalyst due to CO adsorption, and dissolution of Pt lead to lower catalyst activity. Thus, further breakthroughs in electrocatalyst development are needed [14]. Traditionally, a clean Pt surface is key to good electrocatalytic activity. However, many researchers have demonstrated that activity of an electrocatalyst is determined not only by the number of active sites and their structure but also by the nature of the catalyst/electrolyte interface [15,16]. Hence, many researchers have reported the modification of Pt catalyst by altering their nano structured shapes, sizes, composition, and surface by carbon-based materials such as polymers, ionic liquids (IL), and metal organic frameworks [17–20].

IL have been used extensively for metal NPs catalyzed reactions, for stabilizing nanoparticles, and as reaction media [21]. George *et al.* [22] modified a trimetallic Pt-based catalyst (PtNiMo/C) by the SCILL method using either of two hydrophobic IL, 1-butyl-3-methylimidazolium bis(trifluoromethylsulfonyl)imide [BMIM] [NTf_2] or 7-methyl-1,5,7-triazabicyclo [4.4.0] dec-5-

ene bis(pentafluoroethylsulfonyl)imide [MTBD][BETI], with loading amounts ranging between 7-38 wt%. They improved Pt mass activity by 70% when using [MTBD][BETI] and about 50% when using [BMIM] [NTf_2]. However, a decrease in activity was observed when a specific IL loading amount was exceeded, which can be due to a mass transfer related activity drop owing to the high viscosity inherent in most IL. A thin film modified rotating disk electrode (RDE) was used to conduct a background study of the catalysts, and they found suppression of the peak intensities associated with H adsorption and desorption upon increase of the IL loading. However, a small change in the electrocatalytic surface activity area (ECSA) values from 45 to 39 m^2 was observed. In the OH_{ad} regime, the Pt-OH oxidation and reduction peaks were suppressed when the IL loading was increased [22]. They also conducted an accelerated durability test (ADT) for pristine and IL modified catalyst, in which the catalyst was polarized from 0.6 to 1.1 V for 12000 cycles at a scan rate of 50 mV s^{-1}. For the pristine catalyst, after 12000 cycles, about 90% of its ECSA values were retained. However, for the IL modified catalyst, more than 92% of the ESCA was retained. Observation under identical location transmission electron microscopy (TEM) before and after the ADT test revealed that both the modified and unmodified catalyst lost their octahedral shape.

Several researchers have reported that varying the side groups on the cation results in IL with different physicochemical properties, including viscosity, density, thermal stability, and glass transition temperature. Such structural modification opens limitless options of tunability of these materials to specific applications [23–25].

In this work, three tetraalkylphosphonium salts were synthesized owing to their increased hydrophobicity and thermal stability over nitrogen-based ones. High thermal stability is advantageous for operations in high-temperature fuel cells [26,27] as shown in **Table 3.1** with varying alkyl chain lengths on the four-arm bound to the phosphonium core and all were paired with the bis(trifluoromethylsulfonyl)imide (NTf_2^-) anion. The NTf_2 anion was similarly chosen for its hydrophobicity [28]. Two of the three salts are liquids at room temperature even when combined with either NTf_2^- or Br^-.

Table 3.1 Structural specification of phosphonium IL and OIPC

Cation	**Anion**	**Abbreviation**
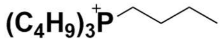	$\overset{-}{N}(SO_2CF_3)_2$	**P$_{4444}$NTf$_2$**
		**P$_{4446}$NTf$_2$**
		**P$_{4448}$NTf$_2$**

3.3 Experimental

3.3.1 Materials and synthesis

All chemicals were used as received without further purification unless indicated otherwise. The Pt/C catalyst (20% on XC-72R carbon black) was purchased from E-Tek. Tributylphosphonium (≥93.5%), 1-bromobutane (≥98%), 1-bromohexane (≥98%), 1-bromooctane (≥98%), 1-bromodecane (≥98%) and lithium bis(trifluoromethylsulfonyl)imide ($LiNTf_2$, 99.95%) were obtained from Sigma-Aldrich. Sulfuric acid (95-98%) was bought from Caledon Laboratories Ltd, and chloroform-D (99.8%) was purchased from Cambridge Isotope Laboratories, Inc. 5% Nafion^{TM} solution was sourced from DuPont, while dichloromethane (≥99.5%), acetone (≥99.5%), and 2-propanol (≥99.5%) were obtained from ACS. Fischer Scientific supplied methanol (99.9%, HPLC Grade). All aqueous solutions were prepared using ultra-pure MilliQ water (>18.2 MΩ cm).

The phosphonium-based IL used in this work were synthesized according to a procedure detailed elsewhere [29]; see also Chapter 2 Section 2.4 [30].

^{1}H NMR was employed to structurally confirm formation and purity of synthesized IL and OIPC using $CDCl_3$ as a solvent. ^{1}H NMR (500 MHz, CDCl3) for **$P_{4444}NTf_2$** - δ 2.15 – 2.06 (m, 8H), 1.48 (m, 16H), 0.99 – 0.91 (t, 12H), **$P_{4446}NTf_2$** δ 2.11 (s, 2H), 2.08 (s, 3H), 1.68 – 1.55 (m, 5H), 1.55 – 1.44 (m, 13H), 1.38 (dt, J = 14.5, 7.2 Hz, 3H), 1.29 (t, J = 3.6 Hz, 2H), 0.98 – 0.83 (m, 12H); **$P_{4448}NTf_2$** δ 2.23 – 2.07 (m, 8H), 1.51 (td, J = 10.7, 5.0 Hz, 16H), 1.37 – 1.24 (m, 8H), 1.03 – 0.95 (m, 9H), 0.92 – 0.85 (m, 3H). See Appendix B for additional details.

The catalyst coated electrodes were prepared by adding 2.0 mg of catalyst to a mixture of 120 μL of H_2O, 30 μL of 2-propanol, and 50 μL Nafion solution and sonicated for 30 min. Subsequently, 3.0 μL of the resulting ink was then drop casted onto a clean, polished 0.071 cm^2 inlaid disk GCE and allowed to dry in air at room temperature.

3.4 Instrumentation

TGA was performed using a thermogravimetric analyzer SDT Q600 TA instrument using an alumina pan. Prior to analysis, a drying step was performed where all samples were heated to 100 °C for 2 h and cooled to room temperature in a desiccator to eliminate mass loss due to water. During analysis, samples were heated in ramp mode from 30 °C to 800 °C at a rate of 10 °C min^{-1} in air.

XRD was used to characterize the catalyst powder using a Rigaku Ultima IV X-ray diffractometer equipped with a Cu-K_{α} radiation of 1.5418 Å. The samples were scanned from 20° to 90° at a power of 40 kV and 44 mA.

IL were structurally confirmed by ^{1}H NMR using a Bruker Avance 500 MHz spectrometer in $CDCl_3$ solvent.

Material thermal behaviour was investigated using a Mettler-Toledo DSC, model DSC1. For details of the procedure see Chapter 2 section 2.5.

Cyclic voltammetric measurements conducted in a conventional three-electrode cell with a Pt wire, glassy carbon electrode (GCE), and saturated calomel electrode (SCE) as counter, working, and reference electrodes, respectively. All electrochemical measurements were performed at ambient temperature (24–25°C) in an N_2 saturated aqueous 1.0 M H_2SO_4 solution using an SP-50 potentiostat controlled by EC-Lab software (Bio-Logic). The working electrode was manually polished using a 0.3 μm alumina suspension (Buehler Inc.) on a polishing pad followed by ultrasonication in an acetone/water bath for 30 min and dried at room temperature.

3.5 Characterization

3.5.1 IL/OIPC characterization

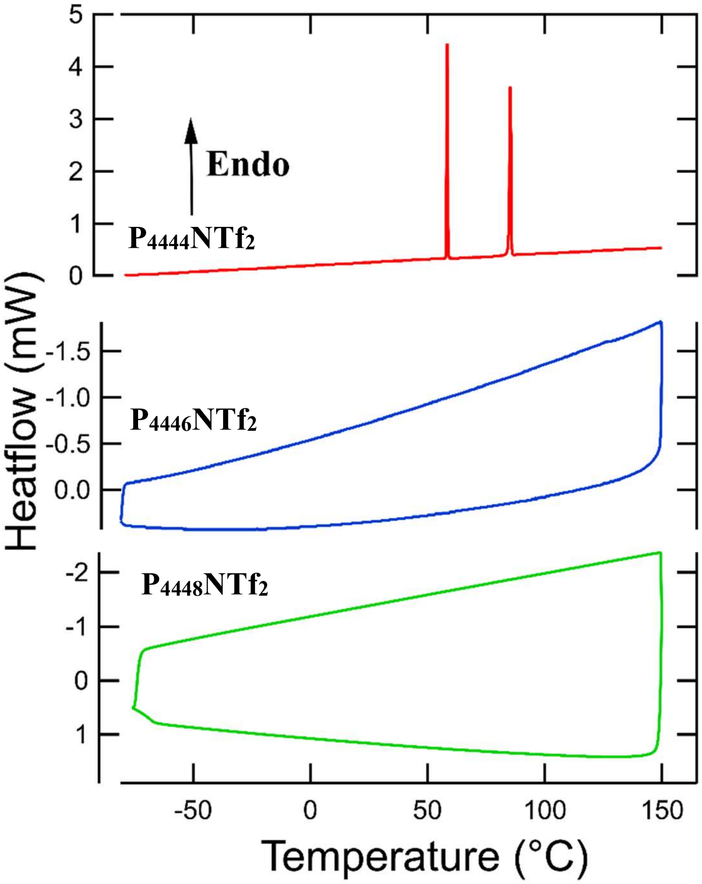

Figure 3.1. DSC thermograms of $P_{4444}NTf_2$ (red), $P_{4446}NTf_2$ (blue), and $P_{4448}NTf_2$ (green) heating from –80 to 150 °C at 2 °C/min.

Thermograms for $P_{4444}NTf_2$, $P_{4446}NTf_2$, and $P_{4448}NTf_2$ have been plotted in Figure 3.1. The $P_{4444}NTf_2$ (red trace), shows two endothermic peaks at 58 and 85 °C corresponding to a solid-solid phase transition (T_{ss}) and melting point (T_m), respectively, making it an OIPC. Interestingly, $P_{4446}NTf_2$ and $P_{4448}NTf_2$ do not show any glass transition (T_g) or cold crystallization temperature (T_{ss}) down to –80 °C.

3.5.2 Catalyst characterization

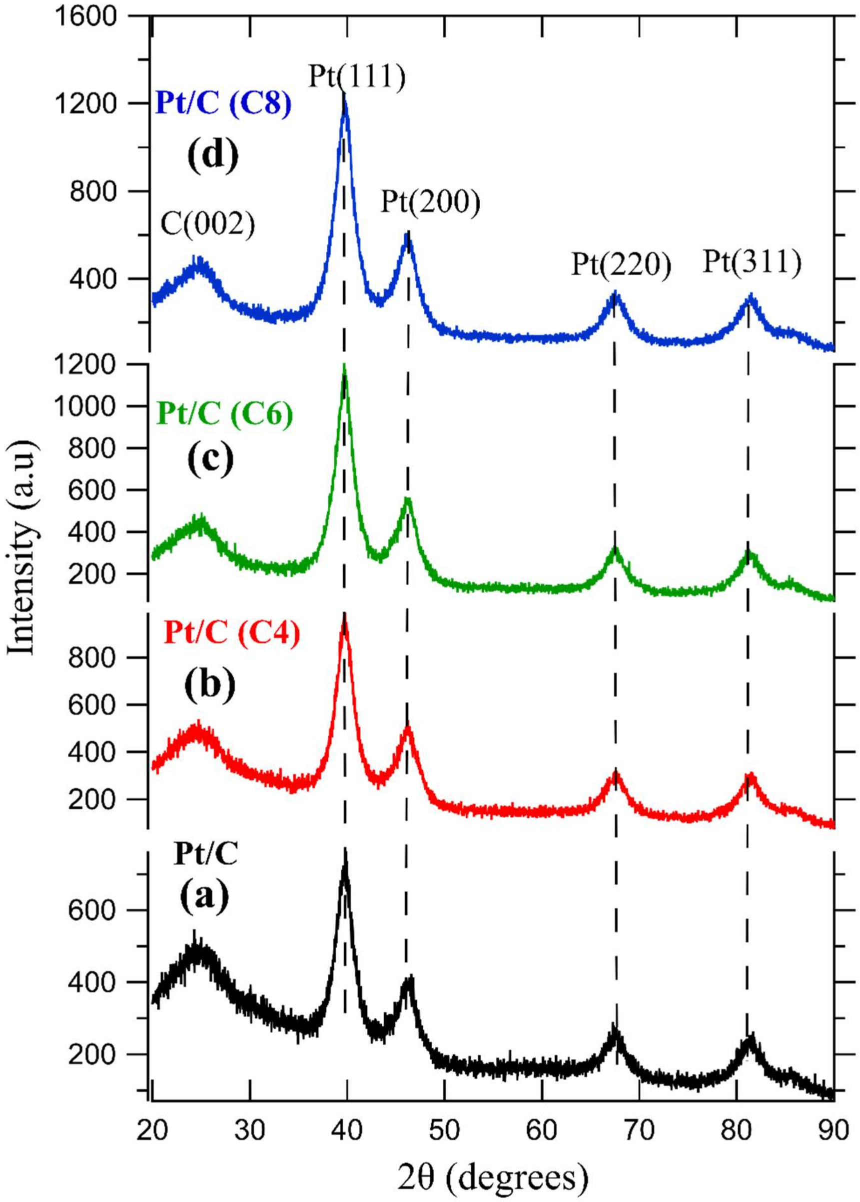

Figure 3.2 X-ray diffraction patterns of (a) Pt/C, (b) 2% $P_{4444}NTf_2$@Pt/C, (c) 2% $P_{4446}NTf_2$@Pt/C and (d) 2% $P_{4448}NTf_2$@Pt/C catalyst.

The XRD patterns of (a) Pt/C, (b) 2% $P_{4444}NTf_2$@Pt/C, (c) 2% $P_{4446}NTf_2$@Pt/C and (d) 2% $P_{4448}NTf_2$@Pt/C have been shown in Figure 3.2. Characteristic 39.51° Pt(111), 46.16° Pt(200), 66.97° Pt(220), and 81.4° Pt(311) peaks associated with the face-centered-cubic (fcc) Pt lattice are present throughout indicating that the Pt crystal structure was not affected by IL/OIPC modification. In addition, a broad distinctive peak of carbon support is seen at 24.78°.

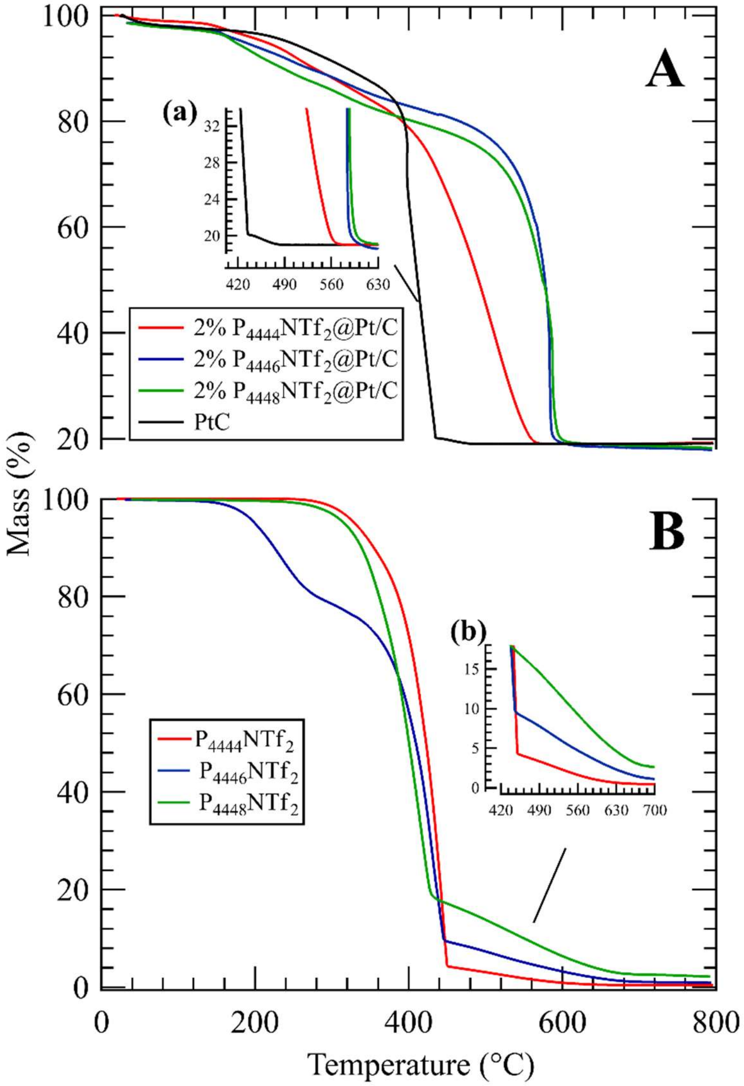

Figure 3.3. TGA curves for [**A**] Pt/C, 2% $P_{4444}NTf_2$@Pt/C, 2% $P_{4446}NTf_2$@Pt/C and 2% $P_{4448}NTf_2$@Pt/C catalyst [**B**] Thermograms for bulk $P_{4444}NTf_2$, $P_{4446}NTf_2$, and $P_{4448}NTf_2$ in air; heating rate 10 °C/min.

As interest in higher-temperature PEM fuel cells grows, it is critical to investigate the thermal stability of carbon-supported Pt catalysts and catalyst materials [31]. Herein, TGA was used to study the thermal stability of IL/OIPC modified catalysts, as well as to investigate the interaction between the IL/OIPC and Pt/C catalyst. Figure 3.3 shows the thermograms obtained for the bare Pt/C and 2% $P_{444*}NTf_2$@Pt/C modified catalysts. These data show that as the temperature was increased from 0-400 °C a slow mass loss was observed which is likely associated with loss of terminal oxygen species on the surface-oxidized carbon support (e.g., $-CO_2H$) along with partial decomposition of the IL/OIPC [30].

Proceeding to higher temperatures above 400 °C, there is a sudden mass loss for the Pt/C catalyst, but gradual mass loss for 2% $P_{4446}NTf_2$@Pt/C and 2% $P_{4448}NTf_2$@Pt/C until 594 °C and 603 °C, respectively, while complete thermal decomposition of 2% $P_{4444}NTf_2$@Pt/C occurred at 559 °C. The thermal decomposition for the OIPC modified catalyst occurred much earlier than for the IL modified catalysts, indicating that the IL are better at thermal stabilization. Results from our previous thermal decomposition data for $P_{4444}NTf_2$@Pt/C have been graphed here for comparison purposes. See Section 2.7 of Chapter 2 [30].

Figure 3.3.**B** depicts thermograms obtained for bulk/single phase IL/OIPC; *i.e*., not layered onto Pt/C catalyst. For the $P_{4444}NTf_2$ a negligible mass loss of ~0.1% and for $P_{4448}NTf_2$ very low mass loss of ~0.5% was observed up to 250 °C, while an abrupt mass loss of ~21% was seen for $P_{4446}NTf_2$ in the region of 100 to 300 °C. $P_{4446}NTf_2$ is the first to start to decompose, at ~200 °C, followed by $P_{4444}NTf_2$ and $P_{4448}NTf_2$ at ~300 °C. The $P_{4446}NTf_2$ undergoes multi-stage decomposition, likely due to residual solvent or reagents. In contrast $P_{4444}NTf_2$ and $P_{4448}NTf_2$ go through single-stage decomposition. The IL and OIPC itself exhibits comparable thermal

behaviour, however when employed as modifiers for Pt/C catalyst IL improves thermal stability of catalyst than the OIPC.

3.6 Electrochemical characterization

Cyclic voltammetry was used to evaluate the electrochemical properties of the catalysts in N_2 saturated 1.0 M H_2SO_4 electrolyte solution. Both the IL/OIPC modified and unmodified Pt/C exhibits the characteristic peaks of Pt in an acidic medium for H^+ adsorption/desorption below ~0 V for the cathodic/anodic scans. At ~0.35 V the anodic peak in the forward scan followed by cathodic peak in reverse scan are associated with oxidation/reduction of quinone moieties on the surface of carbon, which were suppressed after OIPC/IL modification. The H^+ adsorption/desorption peaks were used to calculate the electrochemical active surface areas (ECSA) using equation 6 and are summarized in **Table 3.2.**

$$ECSA = \frac{Q_m N_A}{F d_m} = \frac{Q_m}{e d_m} \tag{6}$$

Where, Q_m is the charge associated with the formation of monolayer, N_A is Avogadro's number, F is the Faraday constant, d_m is the surface metal atom density [35].

The Pt/C catalyst shows the highest ECSA value of 4.53 cm^2, followed by a slight decrease (1.76%) to 4.45 cm^2 for 2% $P_{4444}NTf_2$@Pt/C. For the IL modified catalysts a substantial decrease (9-12%) in ECSA value was observed for 2% $P_{4446}NTf_2$@Pt/C and 2% $P_{4448}NTf_2$@Pt/C to 4.09 cm^2 and 3.99 cm^2, respectively, which indicates that there was signficant blockage of active Pt sites by the IL. A similar loss in ECSA values for Pt/C catalyst was reported by Huang *et al*. [32] and George *et al.* [22] after modification with 10-13% IL.

Catalyst	**ECSA / cm^2**	**Utilization%**
Pt/C	4.5	97
2% $P_{4444}NTf_2$@Pt/C	4.4	95
2% $P_{4446}NTf_2$@Pt/C	4.0	87
2% $P_{4448}NTf_2$@Pt/C	3.9	85

Table 3.2 Calculated ECSA and utilization values for the catalyst

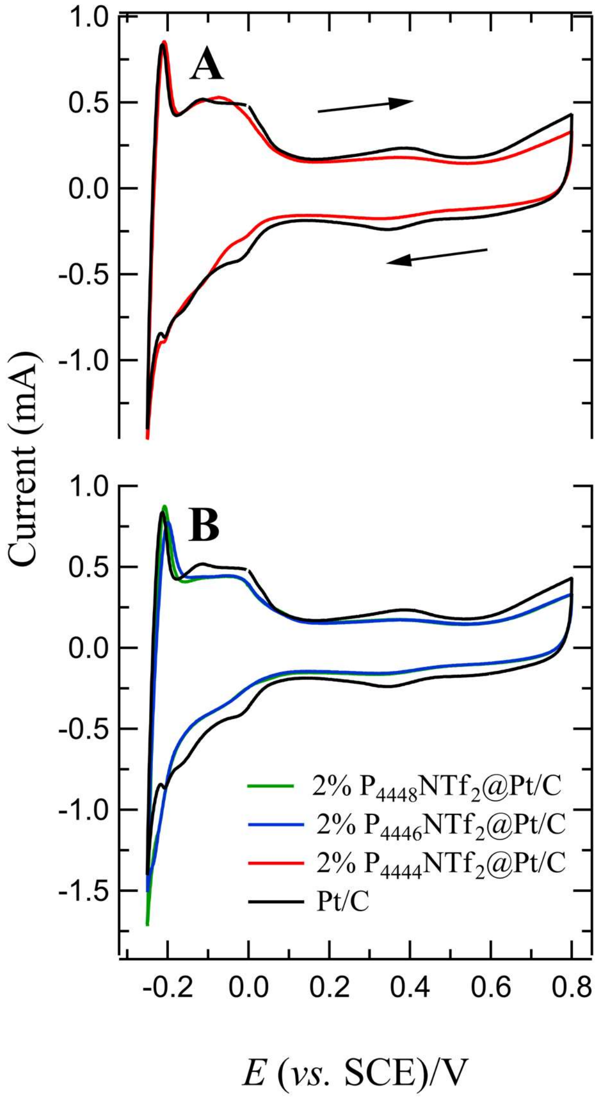

Figure 3.4. Cyclic voltammograms obtained in N_2 saturated 1.0 M H_2SO_4 solution at a scan rate of 100 mV s^{-1} using a GCE modified with [A] 2% $P_{4444}NTf_2$@Pt/C and Pt/C; [B] 2% $P_{4446}NTf_2$@Pt/C and 2% $P_{4448}NTf_2$@Pt/C; Arrows indicate scan directions.

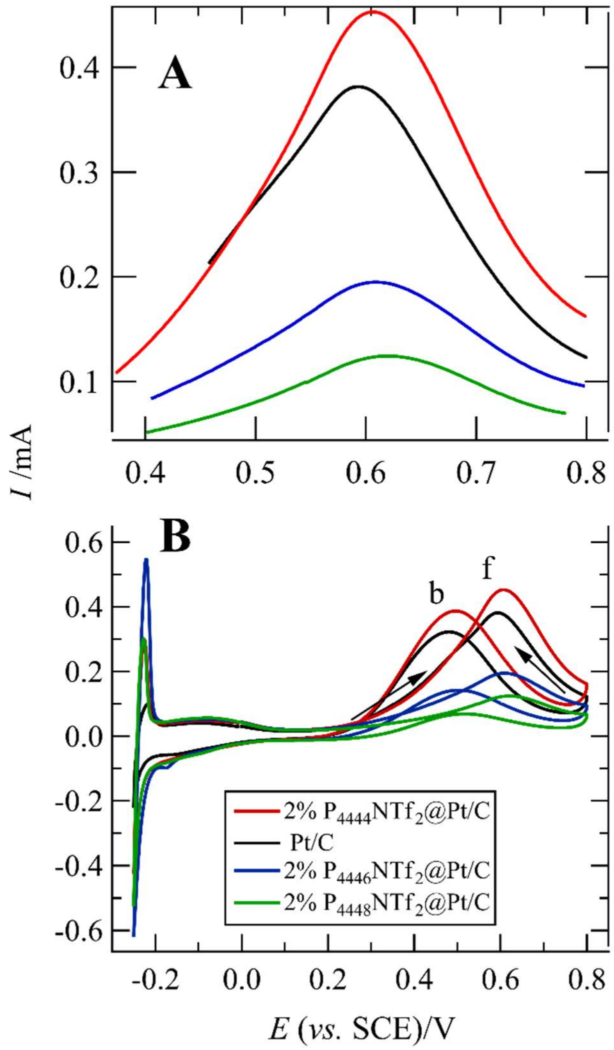

Figure 3.5 Cyclic voltammetry curves of [A] electrooxidation of methanol on Pt/C 2% $P_{4444}NTf_2$@Pt/C, 2% $P_{4446}NTf_2$@Pt/C and $P_{4448}NTf_2$@Pt/C [B] comparison CV for all the catalyst [C] and its forward anodic peak recorded in N_2 saturated 1.0 M H_2SO_4 + 0.1 M CH_3OH aqueous electrolyte solution at scan rate of 10 mV s^{-1}. Arrows indicate scan direction, f and b are forward and reverse peaks.

Figure 3.5 B shows the voltammetric response for electrooxidation of methanol at a scan rate of 10 mV s^{-1} in acid (1.0 M H_2SO_4 + 0.1 M CH_3OH). It exhibits the typical profile of MOR that is characterised by inhibition of the hydrogen adsorption/desorption region from –0.25 V to 0.1 V, followed by an electric double layer until ~0.2 V before the onset of MOR [33]. The onset peak potential for both catalysts was around 0.22 V. In the forward scan for MOR on platinum surfaces, an anodic peak at ca. ~0.6 V was observed which decreases above 0.65 V, due to formation of OH_{ads} or a platinum oxide layer on the NP surface. In the reverse scan the anodic peak at ca. ~0.45 V has been attributed to oxidation of partly oxidized carbonaceous species formed on the Pt surface in the forward scan [34].

The anodic MOR peak has been plotted in **Figure 3.5 A;** the peak currents for 2% $P_{4444}NTf_2$@Pt/C, $P_{4446}NTf_2$@Pt/C, $P_{4448}NTf_2$@Pt/C, and pristine Pt/C were observed to be 0.45, 0.19, 0.12, and 0.38 mA, respectively. Modification using $P_{4444}NTf_2$ generated a roughly 20% increase in MOR peak current, while the IL materials produced a significant decrease. These findings indicate that the electrochemical activity towards MOR increases after OIPC modification but decreases after IL modification. Additionally, a significant decrease in peak current is observed between $P_{4446}NTf_2$@Pt/C and $P_{4448}NTf_2$@Pt/C, indicating the cationic chain length of one arm on the phosphonium core of IL can cause significant changes in electrocatalytic behaviour. These results agree with ECSA values determined above for IL modified catalyst. However, in terms of OIPC it increases activity regardless of the decrease in ECSA, indicative of a co-catalytic effect due to the hydrophobic nature of OIPC

This agrees with a previous report by Zhang *et al* [17] who modified a Pt/C catalyst with a variety of 1-methyl-3-alkylimidazolium bis(trifluoromethanesulfonyl)imide ($[C_nC_1im]$ $[NTf_2]$) IL in which n indicates the length of the alkyl chain bound to the imidazolium ring that was varied from 2-10. They employed the catalyst towards the oxygen reduction reaction (ORR) and observed a similar trend in activity. The maximum improvement in activity was observed with an alkyl chain length with n = 4, which the authors assumed to be a counterbalance between effective suppression of oxygenated species formed on the surface of Pt catalyst and increased passivation of Pt surfaces. Inductively coupled plasma mass spectrometry (ICP-MS) combined with an identical location TEM showed improved electrochemical stability by preventing Pt dissolution [17].

From CV studies it is clear that the electrochemical properties such as ECSA and activity of the catalyst towards methanol oxidation are sensitive to IL/OIPC structure, indicating there are interactions between the IL/OIPC and Pt nanoparticles, which was also inferred from TGA studies from our previous work [30]. **Figure 3.6** shows a possible structure for a IL modified catalyst. The IL is assumed to create a hydrophobic microenvironment on the surface of the catalyst, altering the interfacial surface chemistry. The hydrophobicity after IL/OIPC modification of Pt/C has been studied in our previous work [30]. The hydrophobic environment prevents the leaching or erosion of NPs and protects the active Pt sites from being partially oxidized or forming non-reactive interfering chemical species (e.g.,CO and OH) can be blocked [17,30].

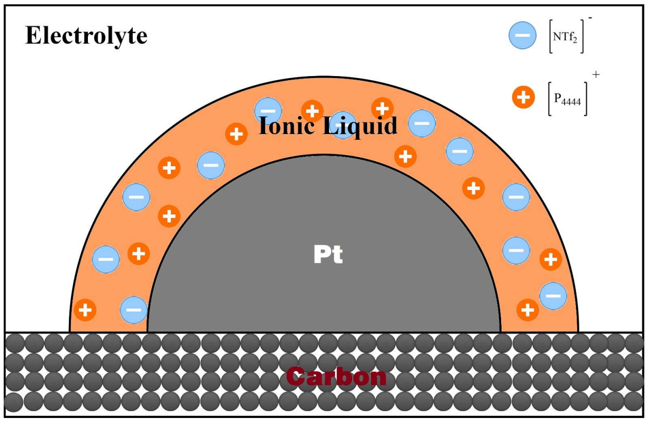

Figure 3.6 Schematic representation of a possible structure of IL modified catalyst

3.7 Conclusion

Herein, three alkylphosphonium based salts with varying chain length of the fourth alkyl group influenced the physicochemical and MOR catalytic properties when applied towards anode surface modification. $P_{4446}NTf_2$ was shown to be an OIPC and when 2% by mass was applied to the surface of a Pt/C commercial catalyst (2% of $P_{4446}NTf_2$@Pt/C) an improved activity towards MOR by 18% in comparison to unmodified Pt/C was observed. The other two salts, $P_{4446}NTf_2$ and $P_{4448}NTf_2$, where shown to be IL and suppressed MOR activity versus pristine Pt/C along with significantly decreasing the ECSA. However, TGA analysis revealed that catalyst modified by IL with longer chain lengths exhibits higher thermal stability.

In this SCILL/SC-OIPC system a small amount of ionic liquid was used; moreover, the enhanced catalytic activity means that less Pt catalyst is required, which will result in a considerable cost reduction. Research on SCILL is still new and more studies are needed for better understanding at a molecular level. The direction of future research is the investigation of catalyst-IL interactions. In addition, the influence of IL loading and IL layer thickness should be analyzed in detail.

3.8 References

[1] A. Yuda, A. Ashok, A. Kumar, A Comprehensive and Critical Review on Recent Progress in Anode Catalyst for Methanol Oxidation Reaction, Catalysis Reviews - Science and Engineering. (2020). https://doi.org/10.1080/01614940.2020.1802811.

[2] P. Majidi, R.M. Altarawneh, N.D.W. Ryan, P.G. Pickup, Determination of the Efficiency of Methanol Oxidation in a Direct Methanol Fuel Cell, Electrochimica Acta. 199 (2016) 210–217. https://doi.org/10.1016/j.electacta.2016.03.147.

[3] T. Iwasita, Electrocatalysis of Methanol Oxidation, Electrochimica Acta. 47 (2003) 3663–3674. https://doi.org/10.1016/S0013-4686(02)00336-5.

[4] J.M. Ogden, M.M. Steinbugler, T.G. Kreutz, Comparison of Hydrogen, Methanol and Gasoline as Fuels for Fuel Cell Vehicles: Implications for Vehicle Design and Infrastructure Development, Journal of Power Sources. 79 (1999) 143–168. https://doi.org/10.1016/S0378-7753(99)00057-9.

[5] S.S. Pethaiah, K.K. Sadasivuni, A. Jayakumar, D. Ponnamma, C.S. Tiwary, G. Sasikumar, Methanol Electrolysis for Hydrogen Production Using Polymer Electrolyte Membrane: A Mini-Review, Energies. 13 (2020). https://doi.org/10.3390/en13225879.

[6] Z.B. Wang, Y.Y. Chu, A.F. Shao, P.J. Zuo, G.P. Yin, Electrochemical Impedance Studies of Electrooxidation of Methanol and Formic Acid on Pt/C Catalyst in Acid Medium, Journal of Power Sources. 190 (2009) 336–340. https://doi.org/10.1016/j.jpowsour.2009.01.008.

[7] A. Sayadi, P.G. Pickup, Evaluation of Methanol Oxidation Catalysts by Rotating Disc Voltammetry, Electrochimica Acta. 199 (2016) 12–17. https://doi.org/10.1016/j.electacta.2016.03.112.

[8] R.N. Singh, Madhu, R. Awasthi, Alcohol Fuel Cells, in: New and Future Developments in Catalysis: Batteries, Hydrogen Storage and Fuel Cells, Elsevier B.V., 2013: pp. 453–478. https://doi.org/10.1016/B978-0-444-53880-2.00021-1.

[9] F. Gao, M. Kabalo, M.S. Rylko, B. Blunier, A. Miraoui, Fuel Cell System, 2013. https://doi.org/10.1007/978-1-4471-5104-3_6.

[10] Corti R. Horacio, Gonzalez R. Ernesto, Direct Alcohol Fuel Cells Materials, Performance, Durability and Applications, 2014. https://doi.org/10.1007/978-94-007-7708-8.

[11] S. Wasmus, A. Küver, Methanol Oxidation and Direct Methanol Fuel Cells: A Selective Review, Journal of Electroanalytical Chemistry. 461 (1999) 14–31. https://doi.org/10.1016/s0022-0728(98)00197-1.

[12] R.M. Altarawneh, T.M. Brueckner, B. Chen, P.G. Pickup, Product Distributions and Efficiencies for Ethanol Oxidation at PtNi Octahedra, Journal of Power Sources. 400 (2018) 369–376. https://doi.org/10.1016/j.jpowsour.2018.08.052.

[13] E.N. el Sawy, P.G. Pickup, Formic Acid Oxidation at Ru@Pt Core-Shell Nanoparticles, Electrocatalysis. 7 (2016) 477–485. https://doi.org/10.1007/s12678-016-0328-8.

[14] X. Ren, Q. Lv, L. Liu, B. Liu, Y. Wang, A. Liu, G. Wu, Current Progress of Pt And Pt-Based Electrocatalysts Used For Fuel Cells, Sustainable Energy and Fuels. 4 (2019) 15–30. https://doi.org/10.1039/c9se00460b.

[15] M.K. Debe, Electrocatalyst Approaches and Challenges for Automotive Fuel Cells, Nature. 486 (2012) 43–51. https://doi.org/10.1038/nature11115.

[16] G.R. Zhang, B.J.M. Etzold, Ionic Liquids in Electrocatalysis, Journal of Energy Chemistry. 25 (2016) 199–207. https://doi.org/10.1016/j.jechem.2016.01.007.

[17] G.R. Zhang, T. Wolker, D.J.S. Sandbeck, M. Munoz, K.J.J. Mayrhofer, S. Cherevko, B.J.M. Etzold, Tuning the Electrocatalytic Performance of Ionic Liquid Modified Pt Catalysts for the Oxygen Reduction Reaction via Cationic Chain Engineering, ACS Catalysis. 8 (2018) 8244–8254. https://doi.org/10.1021/acscatal.8b02018.

[18] I. Do, L.T. Drzal, Ionic Liquid-Assisted Synthesis of Pt Nanoparticles Onto Exfoliated Graphite Nanoplatelets for Fuel Cells, ACS Applied Materials and Interfaces. 6 (2014) 12126–12136. https://doi.org/10.1021/am5012832.

[19] X. Zhao, Y. Hu, L. Liang, C. Liu, J. Liao, W. Xing, Ionic Liquid-Mediated Synthesis of “Clean” Palladium Nanoparticles for Formic Acid Electrooxidation, International Journal of Hydrogen Energy. 37 (2012) 51–58. https://doi.org/10.1016/j.ijhydene.2011.09.075.

[20] R.B. Moghaddam, P.G. Pickup, Mechanistic Studies of Formic Acid Oxidation at Polycarbazole Supported Pt Nanoparticles, Electrochimica Acta. 111 (2013) 823–829. https://doi.org/10.1016/j.electacta.2013.08.098.

[21] A. Banerjee, R.W.J. Scott, Optimization of Transition Metal Nanoparticle-Phosphonium Ionic Liquid Composite Catalytic Systems for Deep Hydrogenation and Hydrodeoxygenation Reactions, Green Chemistry. 17 (2015) 1597–1604. https://doi.org/10.1039/c4gc01716a.

[22] M. George, G.R. Zhang, N. Schmitt, K. Brunnengräber, D.J.S. Sandbeck, K.J.J. Mayrhofer, S. Cherevko, B.J.M. Etzold, Effect of Ionic Liquid Modification on the ORR Performance and Degradation Mechanism of Trimetallic PtNiMo/C Catalysts, ACS Catalysis. 9 (2019) 8682–8692. https://doi.org/10.1021/acscatal.9b01772.

[23] J. Pitawala, A. Matic, A. Martinelli, P. Jacobsson, V. Koch, F. Croce, Thermal Properties and Ionic Conductivity of Imidazolium Bis(Trifluoromethanesulfonyl)Imide Dicationic Ionic Liquids, Journal of Physical Chemistry B. 113 (2009) 10607–10610. https://doi.org/10.1021/jp904989s.

[24] S. v Dzyuba, R.A. Bartsch, Influence of Structural Variations in 1-Alkyl(aralkyl)-3-Methylimidazolium Hexafluorophosphates and Bis(trifluoromethylsulfonyl)imides on Physical Properties of the Ionic Liquids, ChemPhysChem. 3 (2002) 161–166. https://doi.org/10.1002/1439-7641(20020215)3:2<161::AID-CPHC161>3.0.CO;2-3.

[25] M. Yoshizawa, H. Ohno, Triple Ion-Type Imidazolium Salts: A New Class of Single-Ion Conductive Matrix, Ionics. 8 (2002) 267–271. https://doi.org/DOI:10.1007/BF02376078.

[26] T.J. Stockmann, J. Zhang, A.M. Montgomery, Z. Ding, Electrochemical Assessment of Water|Ionic Liquid Biphasic Systems Towards Cesium Extraction from Nuclear Waste, Analytica Chimica Acta. 821 (2014) 41–47. https://doi.org/10.1016/j.aca.2014.03.012.

[27] A.I. Bhatt, I. May, V.A. Volkovich, M.E. Hetherington, B. Lewin, R.C. Thied, N. Ertok, Group 15 quaternary alkyl bistriflimides: Ionic Liquids with Potential Application in Electropositive Metal Deposition and as Supporting Electrolytes, Journal of the Chemical Society. Dalton Transactions. (2002) 4532–4534. https://doi.org/10.1039/b208968h.

[28] K.J. Fraser, D.R. MacFarlane, Phosphonium-Based Ionic Liquids: An Overview, Australian Journal of Chemistry. 62 (2009) 309–321. https://doi.org/10.1071/CH08558.

[29] U. Domańska, M. Wlazło, M. Karpińska, M. Zawadzki, New Ionic Liquid [$P_{4,4,4,4}$][NTf_2] In Bio-Butanol Extraction on Investigation of Limiting Activity Coefficients, Fluid Phase Equilibria. 475 (2018) 89–94. https://doi.org/10.1016/j.fluid.2018.07.028.

[30] A. Suryawanshi, P.G. Pickup, T.J. Stockmann, Organic Ionic Plastic Crystal Surface Modifi-Cation of a Commercial Pt/C Catalyst With Enhanced Formic Acid Oxidation for Fuel Cells, Journal of Ionic Liquids. (2021) (submitted)

[31] J. Melorose, R. Perroy, S. Careas, Fuel Cell Technology Reaching Towards Commercialization, Statewide Agricultural Land Use Baseline 2015. 1 (2015) 1–306. https://doi.org/https://doi.org/10.1007/1-84628-207-1.

[32] K. Huang, T. Song, O. Morales-Collazo, H. Jia, J.F. Brennecke, Enhancing Pt/C Catalysts for the Oxygen Reduction Reaction with Protic Ionic Liquids: The Effect of Anion Structure, Journal of The Electrochemical Society. 164 (2017) F1448–F1459. https://doi.org/10.1149/2.1071713jes.

[33] A.B. Yurtcan, Formic Acid and Methanol Oxidation for Pt/C Catalyst Depending on Rotating Speed, Scan Rate and Concentration, Brilliant Engineering. 1 (2019) 1–4. https://doi.org/10.36937/ben.2020.002.001.

[34] D. Albinsson, S. Bartling, S. Nilsson, H. Ström, J. Fritzsche, C. Langhammer, Shedding Light on CO Oxidation Surface Chemistry on Single Pt Catalyst Nanoparticles Inside a Nanofluidic Model Pore, ACS Catalysis. 11 (2021) 2021–2033. https://doi.org/10.1021/acscatal.0c04955.

[35] J.M. Doña Rodríguez, J.A. Herrera Melián, J. Pérez Peña, Determination of The Real Surface Area of Pt Electrodes by Hydrogen Adsorption using Cyclic Voltammetry, Journal of Chemical Education. 77 (2000) 1195. doi:10.1021/ed077p1195.

Chapter 4

Summary and future work

4.1 Summary

The success of fuel cell technology depends on two aspects, the membrane and the electrocatalyst. In this thesis, we reported how surface modification of the catalyst could result in a highly active electrocatalyst for the oxidation of biofuels.

The second chapter focuses on the development of an anodic catalyst for the oxidation of FA. A high purity aprotic phosphonium-based OIPC synthesized in our lab was used to modify the surface of the catalyst. The synthesized OIPC was characterized using NMR and DSC for its purity and thermal behaviour. The DSC curve for $P_{4444}NTf_2$ OIPC demonstrated two phase transitions (i) below 58 °C and (ii) 58-85 °C. In an SC-OIPC procedure, a very thin layer of OIPC was successfully formed over the surface of the Pt/C catalyst. SEM and optical tensiometer confirmed the OIPC layer formation. The influence of OIPC modification on particle morphology and size was studied using TEM and shows no significant changes. A 2.5× current enhancement towards FA oxidation was achieved by OIPC modification. Background study revealed that the formation of the OIPC layer on the catalyst surface blocks the adsorption of interfering chemical species such as CO and OH. Additionally, although the OIPC was aprotic, an improvement in HER in the region of –0.20 to –0.25 V versus the unmodified commercial catalyst was observed, indicating good solid-state ionic conductivity. The modified catalysts were investigated for thermal stability for applications in high temperature fuel cells as well as to determine Pt loading using TGA analysis.

Which revealed that the presence of OIPC generated a shift in the thermal decomposition of catalyst to higher temperatures. The carbon support and the OIPC itself were also probed.

Next, in Chapter 3, methanol was studied as a fuel due to its high energy density compared to other organic fuels. In this work, $P_{4444}NTf_2$ OIPC as well as two IL were synthesized and used to modify the catalyst's surface. The cationic chain length of one arm on the phosphonium core was varied to six ($P_{4446}NTf_2$) and to eight carbons ($P_{4448}NTf_2$) and paired with the same anion, bis(trifluoromethysulfonyl)imide (NTf_2^-), to achieve IL with different physical and chemical properties. The as-prepared IL existed as liquids and were structurally confirmed using NMR and characterized using DSC; interestingly, none of the IL show a glass transition (T_g) temperature or cold crystallization temperature (T_{ss}) down to –80 °C, meaning they have a broad liquid range. After modification, the background study conducted in an acidic medium showed a slight decrease (~2%) in ECSA values after OIPC modification and a 9-12% decrease after IL modification. It was revealed that the ECSA values are sensitive to the structure of the IL/OIPC, as the ECSA values decrease significantly after elongation of IL chain length.

In terms of MOR, the 2% $P_{4444}NTf_2$@Pt/C exhibited the highest activity, followed by the unmodified commercial Pt/C catalyst. Modification with the $P_{4446}NTf_2$ and $P_{4448}NTf_2$ IL decreased the activity of the catalyst significantly. The maximum activity was achieved with the $P_{4444}NTf_2$ OIPC and the activity tends to decrease with increasing chain length. TGA analysis of the catalysts and IL/OIPC showed that the IL are better at thermally stabilizing catalysts than the OIPC. Although the longer chain IL decreases the activity of the catalyst, it shows an improvement in thermal stability.

In both cases an improvement in activity was observed after OIPC modification, likely due to good solid-state ionic conductivity and ion mobility along grain boundaries of the polycrystalline aprotic OIPC, which impacts the microenvironment around the Pt/OIPC interface. Overall, the proposed SC-OIPC is a cost reductive technique since a major improvement in activity of catalyst is achieved that equals or exceeds the performance of other electrocatalyst formulations that employ far more Pt, lowering the catalyst's overall cost. This could be a game-changing, ground-breaking achievement in fuel cell research. Together, these results should be of considerable interest for next generation fuel cell technologies, electrocatalysis, and materials chemistry communities.

4.2 Future work

These highly impactful findings towards fuel cell electrocatalyst modification demonstrate the continued utility of IL and OIPC materials and can serve as a springboard for more in-depth research. In this regard, we present a list of study subjects that are currently being investigated or are being considered for future research.

1. Investigating the electrochemical activity and durability of IL/OIPC modified catalysts using a 9-anode PEM cell. Accelerated degradation test coupled with identical location TEM to investigate catalyst stability for practical device applications.
2. To further understand the boosting effect of IL/OIPC modification by probing the interaction of OIPC/IL over the catalyst surface using AFM and Ellipsometry.
3. To create a porous, thin-film by polymerizing IL with embedded Pt NPs, without any carbon support and analyze its electrochemical behaviour using scanning electrochemical

microscopy (SECM); testing them *in operando* as anodic catalysts for the biofuel oxidation reaction.

Appendix

Appendix A

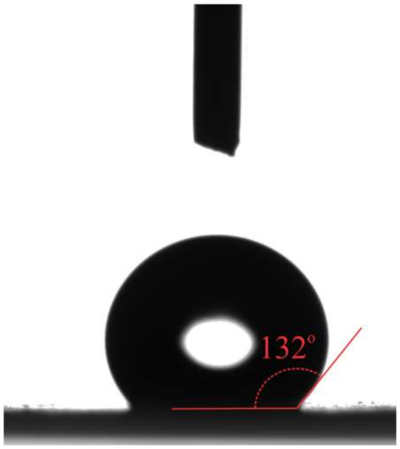

Figure A1: Photo of static water-contact-angle measurements of a $P_{4444}NTf_2$ coated glass slide.

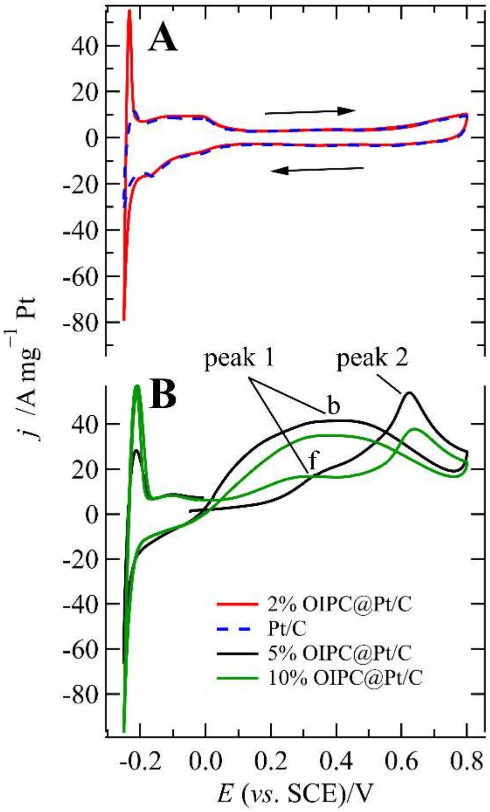

Figure A2. CVs at a scan rate of 10 mV s^{-1} for [**A**] unmodified Pt/C and 2% OIPC@Pt/C modified catalysts, recorded in N_2 saturated 1.0 M H_2SO_4 electrolyte, as well as [**B**] after 0.1 M HCOOH was added for 5 and 10% OIPC@Pt/C as indicated inset. Here f = forward wave and b = backward.

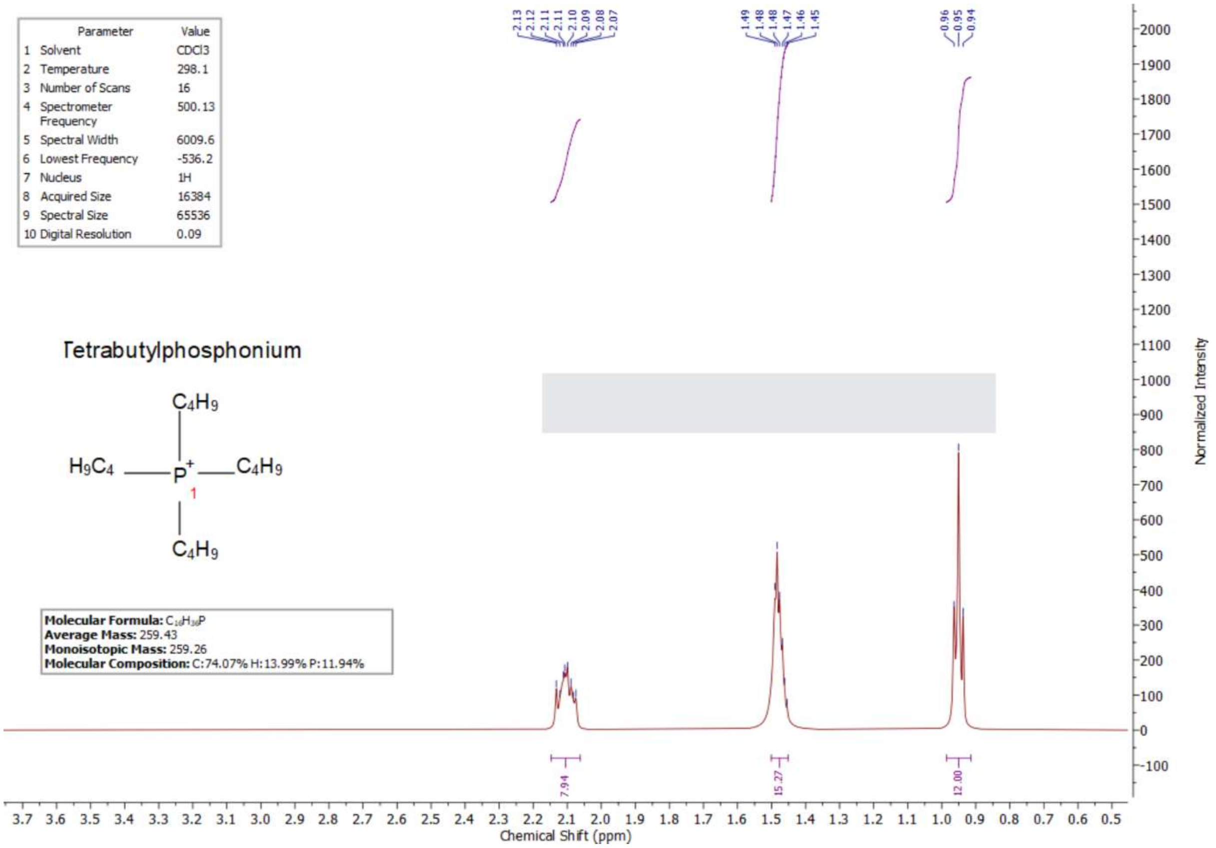

	Parameter	Value
1	Solvent	CDCl3
2	Temperature	298.1
3	Number of Scans	16
4	Spectrometer Frequency	500.13
5	Spectral Width	6009.6
6	Lowest Frequency	-536.2
7	Nucleus	1H
8	Acquired Size	16384
9	Spectral Size	65536
10	Digital Resolution	0.09

Molecular Formula: $C_{16}H_{36}P$
Average Mass: 259.43
Monoisotopic Mass: 259.26
Molecular Composition: C:74.07% H:13.99% P:11.94%

Figure A3: ^{1}H NMR of $[P_{4,4,4,4}]$ $[NTf_2]$ in $CDCl_3$.

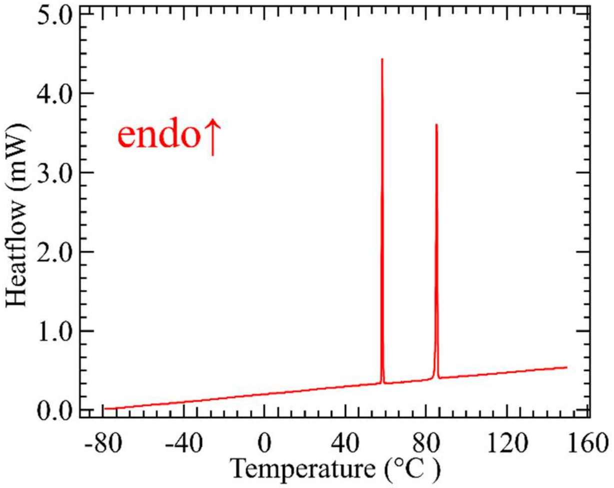

Figure. A4 DSC thermogram of the ionic liquid $[P_{4,4,4,4}]$ $[NTf_2]$, heating from –80 to 150 °C at 2 °C/min.

Table A1: Pt loading results obtained from TGA and SEM-EDX analysis

Catalyst	%Pt loading		
	Calculated	EDX	TGA
Pt/C	20.0	19.8	19.03
2% OIPC@Pt/C	19.6	19.6	19.04

Appendix B

Figure B1: ^{1}H NMR of $[P_{4,4,4,6}]$ $[NTf_2]$ in $CDCl_3$.

Figure B2: ^{1}H NMR of $[P_{4,4,4,8}]$ $[NTf_2]$ in $CDCl_3$.

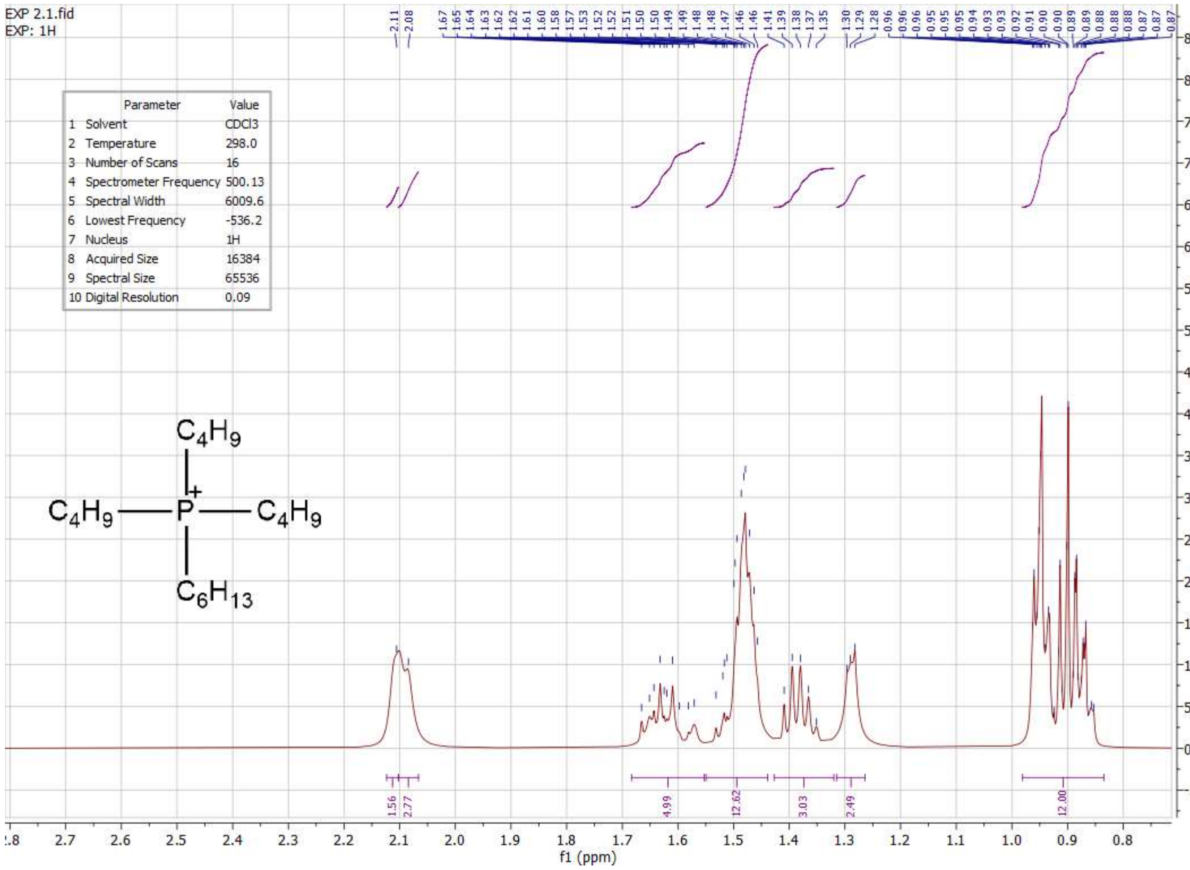

	Parameter	Value
1	Solvent	CDCl3
2	Temperature	298.0
3	Number of Scans	16
4	Spectrometer Frequency	500.13
5	Spectral Width	6009.6
6	Lowest Frequency	-536.2
7	Nucleus	1H
8	Acquired Size	16384
9	Spectral Size	65536
10	Digital Resolution	0.09

Figure B1: ^{1}H NMR for [$P_{4,4,4,6}$] [NTf_2] IL in $CDCl_3$.

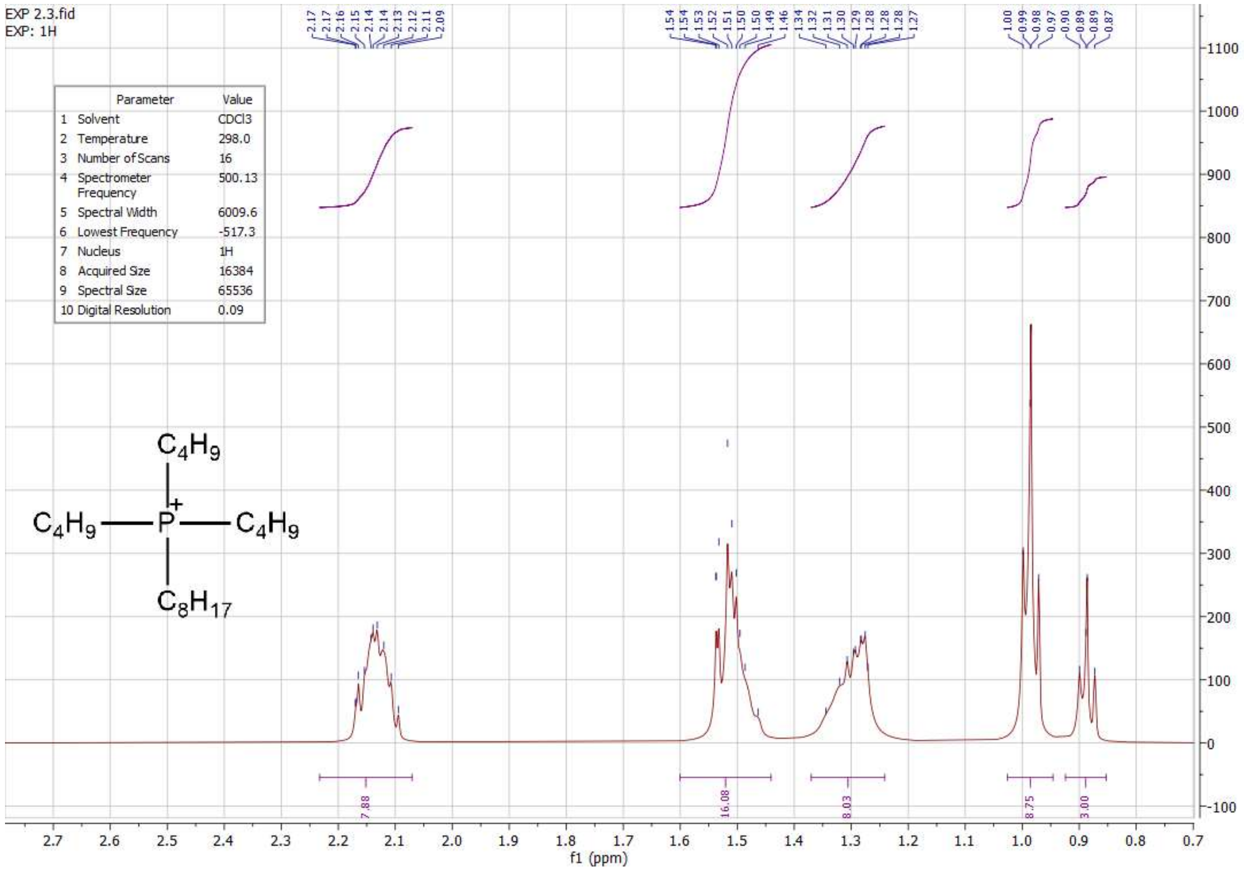

Parameter	Value
1 Solvent	CDCl3
2 Temperature	298.0
3 Number of Scans	16
4 Spectrometer Frequency	500.13
5 Spectral Width	6009.6
6 Lowest Frequency	-517.3
7 Nucleus	1H
8 Acquired Size	16384
9 Spectral Size	65536
10 Digital Resolution	0.09

Figure B2: ^{1}H NMR for [$P_{4,4,4,8}$] [NTf_2] IL in $CDCl_3$